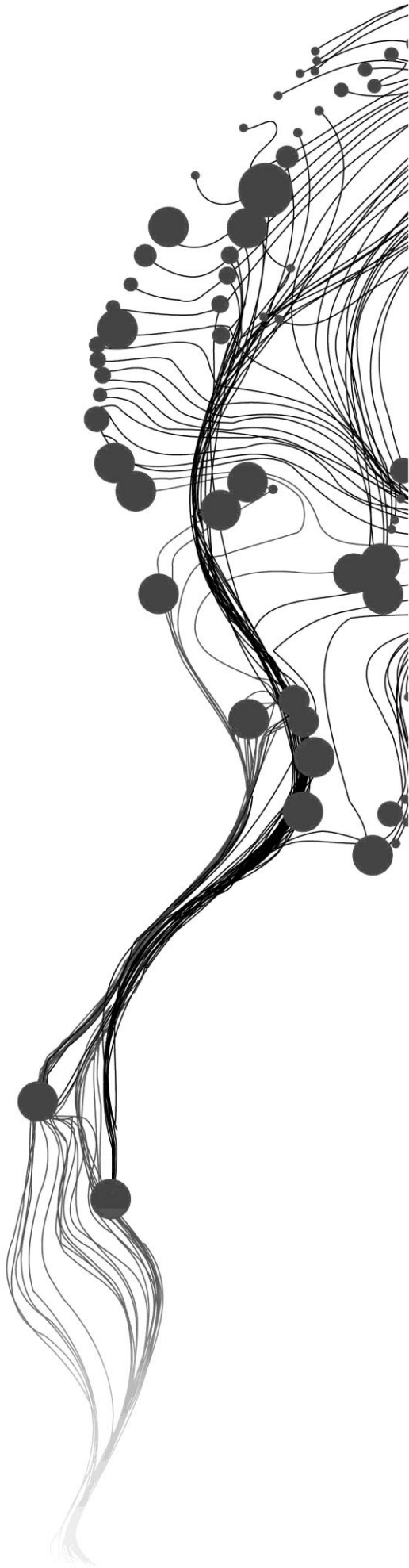


# **Analysis of Sentinel-1 SAR data for mapping standing water in the Twente region**

CHANG LIU  
February, 2016

SUPERVISORS:  
Dr. Ir. Rogier van der Velde  
Dr. Zoltán Vekerdy





# **Analysis of Sentinel-1 SAR data for mapping standing water in the Twente region**

**CHANG LIU**

Enschede, The Netherlands, February, 2016

Thesis submitted to the Faculty of Geo-Information Science and Earth Observation of the University of Twente in partial fulfilment of the requirements for the degree of Master of Science in Geo-information Science and Earth Observation.

Specialization: Water Resource and Environmental Management

**SUPERVISORS:**

Dr. Ir. Rogier van der Velde

Dr. Zoltán Vekerdy

**THESIS ASSESSMENT BOARD:**

Dr. Ir. C. van der Tol (Chair)

Dr. Tao Wang (External Examiner, Capital Normal University)

#### DISCLAIMER

This document describes work undertaken as part of a programme of study at the Faculty of Geo-Information Science and Earth Observation of the University of Twente. All views and opinions expressed therein remain the sole responsibility of the author, and do not necessarily represent those of the Faculty.

# ABSTRACT

The Sentinel-1 mission is expected to deliver a wealth of data and imagery. As the first member of the constellation of two satellites, the Sentinel-1A with C-band was launched on 3<sup>rd</sup> April, 2014. It has dual-polarization capability (HH+HV or VV+VH) which can provide more ground surface information. This study aims to analyse Sentinel-1 SAR data for its potential to map standing water in agricultural fields over the Twente region.

Level-1 Ground Range Detected (GRD) Sentinel-1 C-band (5.405 GHz) data collected in the Interferometric Wide swath (IW) mode were used to develop a procedure for reliable processing of the Sentinel-1 SAR images. There are 73 SAR images have been collected during the period from October 2014 to September, 2015. Those series SAR images were utilized to investigate the multi-temporal backscatter properties (e.g. mean and standard deviation) for different land cover across the Twente region. Based on the backscatter temporal variability, multi-temporal backscatter observations can be used to classify the agricultural field from forest, urban, open water body and grassland. However, because of the effect of surface roughness, soil moisture and vegetation growth, winter wheat and corn field are difficult to distinguish.

Fieldwork has been done from 17<sup>th</sup> September, 2015 to 2<sup>nd</sup> October, 2015 to find the standing water in agricultural fields. At the same time, the landscape changes and agricultural activities were also recorded in order to analyse backscatter changes with respect to human activities. There are 6 fields had been visited including two grassland, two corn fields and two winter wheat fields. Only one winter wheat fields (No.7 field) had obvious surface water. Standing water in one grassland (No.4 field) spread as mosaic under the thick grass.

In addition, backscatter changes in response to atmospheric forcings (e.g. rainfall) and land surface conditions (e.g. soil moisture) were analyzed for the individual fields with different land covers (e.g. grassland, winter wheat, corn) to find the possible periodically standing water. Among all the possible influence factors, soil moisture is the dominant factors in backscatter changes. However, standing water is difficult to delineate from the Sentinel-1 images due to the uncertainties. Those uncertainties include different surface conditions in each agricultural field, soil moisture, vegetation characteristics and agricultural activities. Those factors vary from temporal and spatial scale, like farming practices and atmospheric forcings.

Keywords: Standing water, Agricultural fields, Sentinel-1, Backscatter analysis

## ACKNOWLEDGEMENTS

First and foremost, I must show my very profound gratitude to my parents for their support and always encourage me to do my studies.

Then I would like to express my sincere thanks to my first supervisor Dr. Rogier van der Velde for his advices, suggestions, continuous guidance throughout the thesis work and even guide in my thesis writing. I would also like to thank my second supervisor Dr. Zoltan Vekerdy for his precious time, new thoughts, advices, guidance and comments to improve the thesis.

I would also like to thank my teacher Mrs. Wang (Lichun Wang) for helping me with IDL coding, and Phd student H.F. Benninga for helping me solve the problems during my thesis work.

Finally, I would like to say big thank you to my friends for supporting and encouraging me to finish my study, researching and writing this thesis. Thank you.

.

# TABLE OF CONTENTS

---

1.	Introduction .....	1
1.1.	Background.....	1
1.2.	Open water detection using SAR .....	2
1.2.1.	Overview of spaceborne SAR Sensors.....	2
1.2.2.	Detection of open water .....	2
1.3.	Research problem .....	3
1.4.	Objectives and research questions .....	4
1.4.1.	General objective.....	4
1.4.2.	Specific objectives.....	4
1.4.3.	Research questions .....	4
1.5.	Thesis and research structure .....	4
2.	Study area and data.....	6
2.1.	Study area .....	6
2.2.	Sentinel-1 data .....	6
2.3.	Rainfall data.....	7
2.4.	Soil moisture data .....	7
2.5.	Vegetation index .....	8
2.6.	Land cover data.....	8
3.	Methodology.....	11
3.1.	Fieldwork.....	11
3.2.	Identification of agricultural areas .....	11
3.3.	Standing water detection and verification.....	13
4.	Fieldwork.....	14
4.1.	Description of the observed fields .....	14
4.2.	Landscape changes during the fieldwork.....	14
5.	Sentinel-1 data Pre-processing .....	18
5.1.	Terrain correction .....	18
5.2.	View angle review .....	19
5.3.	Speckle filter.....	19
6.	Backscatter analysis.....	22
6.1.	Image based backscatter analysis.....	22
6.2.	Field-scale backscatter changes and standing water detection.....	25
6.3.	Temporal verification.....	27
6.3.1.	Rainfall and soil moisture trend .....	27
6.3.2.	NDVI for agricultural fields .....	28
6.3.3.	Periodically standing water in winter wheat field .....	29
6.3.4.	Periodically standing water in grassland .....	30
7.	Conclusion and recommendation .....	32
7.1.	Conclusions.....	32
7.2.	Limitations and recommendations .....	32

## LIST OF FIGURES

---

Figure 1 Flowchart of research method .....	5
Figure 2 On the left: map of Netherlands with the Twente region highlighted. On the right: Google Earth image of the area covered by the soil moisture stations and weather monitoring stations belong to the Royal Netherlands Meteorological Institute (KNMI). .....	6
Figure 3 Daily rainfall from 2010 to 2014 in Twente KNMI monitoring station as highlight in Figure 1 .....	7
Figure 4 Vegetation Index (NDVI) for observed fields provided by Groenmonitor website ( <a href="http://www.groenmonitor.nl/groenindex">http://www.groenmonitor.nl/groenindex</a> ) .....	8
Figure 5 Land cover map of study area available on the websit of Overijssel by the Province of Overijssel ( <a href="http://gisopenbaar.overijssel.nl/viewer/app/bodematlas/v1">http://gisopenbaar.overijssel.nl/viewer/app/bodematlas/v1</a> ) .....	9
Figure 6 Scattering mechanisms ( <a href="http://imaging.geocomm.com/faq/">http://imaging.geocomm.com/faq/</a> ) .....	11
Figure 7 The distribution of land cover classes in the backscatter temporal variability and long- term coherence feature space (Bruzzone et al., 2004) .....	12
Figure 8 Landscape in each observation field. ....	14
Figure 9 Sentinel-1 data processing steps .....	18
Figure 10 Filter results of VH-polarized SAR images acquired on 16-09-2015 .....	20
Figure 11 Backscatter (in dB) for RGB colour composite (Green--VH polarization; Red and Blue- -VV polarization) at different dates .....	21
Figure 12 Backscatter temporal variability calculated by different estimators for RGB colour composite (Green--VH polarization; Red and Blue--VV polarization) at different dates : (a) Saturation backscatter; (b) Maximum-Minimum Ratio in dB; (c) Logarithmic measure based on normalized Standard deviation; (d) Normalized standard deviation .....	22
Figure 13 Backscatter statistics result for RGB colour composite (Green--VH polarization; Red and Blue--VV polarization): (a) mean backscatter (in dB); (b) standard deviation of backscatter (in dB) .....	23
Figure 14 Backscatter statistics for different land cover classes, (a) Standard deviation for VH and VV polarization, (b) Average backscatter for VH and VV polarization. ....	25
Figure 15 Backscatter changes of different land cover .....	26
Figure 16 Daily rainfall data collected from Twente station, and the soil moisture data averaged from the 20 soil moisture network stations in Tewnte from October 2014 to September 2015. .....	27
Figure 17 NDVI for corn fields, winter wheat field and grassland. ....	29
Figure 18 Soil moisture with backscatter of No.9 field and daily rainfall derived from Twente station. ....	30
Figure 19 Soil moisture with backscatter [dB] of No.4 field and daily rainfall derived from Twente station .....	31

## LIST OF TABLES

---

Table 1 Characteristics of the Sentinel-1 Interferometric Wide swath mode nominal measurement modes (Torres et al., 2012; Sentinel-1 Team, 2013).....	7
Table 2 Backscatter estimators.....	12
Table 3 Landscape changes in No.7 observed fields.....	15
Table 4 Landscape changes in No.4 observed fields.....	16
Table 5 Landscape changes in No.3 observed fields.....	17
Table 6 Dynamic range of backscatter in different land cover .....	25



# 1. INTRODUCTION

## 1.1. Background

Standing water occurs as a result of heavy or persistent rainfall, flooding by rivers and lakes, water table rise, snowmelt above frozen soils, or artificially as a result of the construction of reservoirs. Standing water on agricultural fields is likely to influence the crop growth conditions, lead to poor soil aeration, increases the pH of acid soils and decreases the pH of alkaline soils. When standing water occurs, some degree of damage to the crop is usually inevitable. The extent of the damage depends on the crop type, its growth stage, the duration of standing water, and temperatures during standing water. Damage occurs because water logged soils are quickly depleted of oxygen in the root zone, and the supply of oxygen to water logged soil is severely limited. Most crops require oxygen for normal metabolism, growth and development. Furthermore, standing water frequently results in higher levels of plant diseases that reduce yields. Berning et al. (2000) showed that the depth and duration of standing water were two dominant factors leading to the decrease of sugar-cane harvest in the Mfolozi floodplain. Furthermore, due to the fact that the soil is moist and soft under the conditions of standing water, many agricultural activities with respect to ploughing, seeding, and harvesting can be also affected.

In recent years, space-borne remote sensing has widely been recognized as a technique that is beneficial for quantitative estimation of flooded extent. Remote sensing images from optical, thermal, and microwave wavelengths can be used for standing water delineation. However, the major challenge in the application of visible or thermal imagery to standing water mapping is that flood events are often associated with cloud cover, particularly in the small and medium-size areas (Ticehurst et al., 2009; Schlaffer et al., 2015). Moreover, vegetation canopies also limit the applicability of these sensors to map standing water extent. Water cannot be detected when the surface ponding is in the shadow of the vegetation cover. On the other hand, optical imagery is easy to interpret, and the extraction of the standing water area from optical imagery is generally more straightforward than from radar imagery (Schumann et al., 2009). Compared with optical sensors, microwaves sensors have longer wavelengths varying from less than one centimeter to one meter (or frequencies from 89 GHz to 0.3 GHz) (Ticehurst et al., 2009). Synthetic Aperture Radar (SAR) is an active microwave remote sensing technique with the capability of being independent of solar illumination. Due to the wavelength, the signal has limited interaction with the droplets in the cloud without obscuring observations (G. Schumann et al., 2009). More importantly, because of SAR systems are capable of acquiring observations in both day-time and night-time and even under extreme weather conditions, it becomes the most suitable instruments for high-resolution flood mapping from space (Hostache et al., 2012). In general, the return signals of SAR are influenced by the view angle of the sensor, the material of the reflecting objects and the surface roughness as well as the frequency and polarization (Gstaiger et al., 2012; Townsend & Walsh, 1998). Nowadays more and more microwave satellites are available with high resolution, such as TerraSAR-X, COSMO-SkyMed, RADARSAT-2 and Sentinel-1. Also for given the rapid flood recession in small to medium sized catchments, the delineation of standing water extent and systematic monitoring seems realistically more feasible with SAR imagery (G. J.-P. Schumann & Moller, 2015).

## 1.2. Open water detection using SAR

In this section, satellites for detecting flood extent and methods for delineating flood area are reviewed.

### 1.2.1. Overview of spaceborne SAR Sensors

Since the launch of the first radar satellite SEASAT, in 1978, microwave sensors have increasingly been used for flood delineation. The two European Remote Sensing Satellites, ERS-1, and ERS-2 were launched in 1991 and 1995, respectively. These two ESA satellites were in charge of collecting a wealth of valuable data associated with land surface, ocean, polar caps, and natural disasters (ERS overview). The Advanced Synthetic Aperture Radar (ASAR) on the ENVISAT satellite is an improved version of the sensors on ERS by offering five polarization configurations: HH, VV, HH/VV, HV/HH, VH/VV (Henry et al., 2006). In addition, it enhances the capabilities in terms of coverage, range of incidence angles, polarisation, and modes of operation (ASAR - Earth Online). With a moderate resolution of 30 m, ENVISAT has been used for extracting the standing water extent in rural areas (Kuenzer et al., 2013; Matgen et al., 2011). Unfortunately, the ENVISAT mission ended on 8<sup>th</sup> April, 2012 following from the unexpected loss of contact with the satellite. More recently, a number of SAR sensors with high resolution as fine as 3 m or higher are available for both urban and rural flood mapping studies, such as RADARSAT-2 (C-band), TerraSar-X (X-band), and four COSMO-SkyMed (X-band) satellites (Gstaiger et al., 2012; Pulvirenti et al., 2011). Compared to those high resolution sensors, Sentinel-1 has the higher temporal resolution due to its configuration: two satellites work at the same time increasing the re-visit time to maximum 5 days. Moreover, Sentinel-1 can cover large areas and the images are free to the public. Gstaiger et al. (2012) showed that TerraSAR-X data could provide water mask with very high spatial detail and accuracy, but covers only small areas depending on the acquisition mode.

The Sentinel-1 mission is expected to deliver a wealth of data and imagery that are central to the Copernicus joint initiative of the European Commission (EC) and European Space Agency (ESA). As the first member of the constellation of two satellites, the Sentinel-1A was launched on 3<sup>rd</sup> April, 2014 with a revisit cycle of 12 days. Sentinel-1 includes C-band imaging Synthetic Aperture Radar (SAR) in four exclusive imaging modes: Interferometric Wide Swath Mode (IW), Wave-Mode (WM), Strip Map Mode (SM), and Extra-Wide Swath Mode (EW). With different resolutions (from 5 m to 40 m) and coverage (from 80 km to 400 km), the four modes can meet the demanding image quality and swath width requirements (Sentinel-1 User handbook, 2013).

### 1.2.2. Detection of open water

The features of standing water or surface conditions in SAR imagery are the result of different factors, including acquisition characteristics (wavelength, incidence angle, polarization), soil moisture, vegetation characteristics, and soil surface conditions (roughness and inundation) (Hostache et al., 2012). For transmission/acquisition characteristics, polarization refers to the direction of the electric field vector of the transmitted/received beam with respect to the horizontal direction. Sentinel-1 provides selectable polarization capability: selectable single polarization (VV or HH) for Wave-Mode and selectable dual-polarization (VV+VH or HH+HV) for the other three modes (Attema et al., 2009). Previous studies conclude that the dual-polarization data HH + HV gave the most informative result for flood mapping (Matgen et al., 2011). As an alternative, the single polarization model HH can also be used for flood mapping, better than VV, or cross-polarized used individually, without HH, since the HH-polarized data is less influenced by surface roughness on open water caused by waves (Henry et al., 2006).

During the last decade, many methods have been developed for flood mapping with SAR images. From a general perspective, these methods can be divided into two categories: single-image analysis

and change detection approaches (Schlaffer et al., 2015). Single-image analysis is performed without considering how surface ponding changes over time. Schumann et al. (2009) investigated the use of several single-image analysis methods, like visual interpretation, image texture analysis, histogram thresholding, and edge detection approach. The authors concluded that flood mapping with a multi-algorithm including visual interpretation, image texture analysis, histogram thresholding, and edge detection approach integrated method, gave better result than using only a single algorithm. Similar results can be found in the work by Di Baldassarre et al., (2009b), who used the aforementioned four methods together with an Euclidean distance method to get inundation maps derived from both coarse resolution (150 m) images (ENVISAT ASAR WS) and high resolution (12.5 m) satellite images (ERS-2 SAR). Their results demonstrated that visual interpretation and image texture analysis were largely rely on the sensitivity of feature differences in the human visual system. Hence, interpreting the flood boundary visually depends much on the operator's ability of distinguishing different grey scale tones and their knowledge of the flood process. In another study, a thresholding technique has been viewed as an efficient flood mapping method (Schumann et al., 2009). In general, thresholding is a key point in the histogram-based approach and pattern recognition (Bazi et al., 2007). Gstaiger et al.,(2012) compared three simple approaches to derive standing water areas from TerraSAR-X data. Two methods are pixel-based and use histogram-based empirically defined grey-level thresholds, as well as a homogeneity criterion for classification. The third approach is object-based by using empirically chosen values and thresholds for classification with several segments attributes, such as grey value, shape, texture and relations to neighbouring objects (Gstaiger et al., 2012). Those attributes were analysed and taken into consideration in a decision tree to classify water and non-water areas. Kuenzer et al. (2013) employed 60 ENVISAT ASAR Wide Swath mode images with simple, empirically chosen thresholds to understand the flood inundation pattern in the Mekong Delta during 2007-2011. Furthermore, hybrid methods have been proposed by combining thresholding algorithms with other image analysis approaches, e.g. region growing method (Giustarini et al., 2013; Matgen et al., 2011). From their studies, a threshold was used to extract the core of the water bodies from SAR data and to identify the seed region for the region growing step. Then neighbouring pixels were identified which have similar backscatter values to those in the seed region. Moreover, a fuzzy logic was used to improve the accuracy of flood mapping by taking into account ancillary hydraulic characteristic and contextual information (Pulvirenti et al. 2011). In order to separate the permanent and the temporarily flooded areas and to overcome the disadvantages of single-image analysis methods, much attention has been devoted to integrating change detection approaches to the aforementioned single-image analysis methods.

### 1.3. Research problem

Due to the fact that in the summer the potential evapotranspiration ( $ET_p$ ) is higher than the precipitation, but in the winter the precipitation exceeds the  $ET_p$ , the surface and subsurface runoff, standing water events occur at agricultural fields. As the previous studies introduced in Section 1.2, the potential of mapping the extent of inundation in floodplains using satellite images is widely acknowledged. However, various problems are involved in standing water mapping with satellite remote sensing imagery at field scale. For instance, standing water on agricultural fields is patchy, leading to the mixing of signals from land and open water both at the optical and the radar wavelengths. Also, the presence of vegetation can obscure observation of surface ponding in fields. Furthermore, due to the agricultural seasonality, the standing water situation is different on fields with different crop within one image. These features add uncertainty to the standing water mapping.

## 1.4. Objectives and research questions

### 1.4.1. General objective

This study aims to analyse Sentinel-1 SAR data for its potential to map standing water in agricultural fields over the Twente region.

### 1.4.2. Specific objectives

In order to achieve the general objective of this research three specific objectives are formulated as follows.

- 1) To develop a procedure for reliable processing of the Sentinel-1 SAR images;
- 2) To investigate the multi-temporal backscatter properties (e.g. mean and standard deviation) for different land cover across the Twente region;
- 3) To analyse the backscatter changes for the individual fields with different land covers (e.g. grassland, winter wheat, corn) in response to atmospheric forcings (e.g. rainfall) and land surface conditions (e.g. soil moisture).

### 1.4.3. Research questions

The questions related to the aforementioned sub-objectives are illustrated as follows.

- Can the raw Sentinel-1 data be processed to reliable SAR imagery?
- How do the multi-temporal Sentinel-1 backscatter properties (e.g. mean and standard deviation) vary with land cover?
- Can standing water within agricultural field be detected from a series of Sentinel-1 images?

## 1.5. Thesis and research structure

This thesis is organized in seven chapters. Study area and main dataset, like Sentinel-1 SAR images and ancillary dataset are introduced in Chapter 2. Chapter 3 describes the methodology, which is used to analyze Sentinel-1 SAR data for its potential to map standing water within agricultural fields. Chapter 4 present the fieldwork observation and landscape. In Chapter 5, Sentinel-1 images pre-processing steps and results are described in details. Chapter 6 contains the backscatter analysis with respect to image-based backscatter analysis and field-scale backscatter change. Based on those analysis, possible periodically standing water will be detected from the backscatter changes throughout the study period. In addition, ancillary data like in-situ rainfall, soil moisture and NDVI are used to verify the possible standing water. Finally, in Chapter 7, conclusion and recommendation are drawn. An overview of the research method is showed in Figure 1.

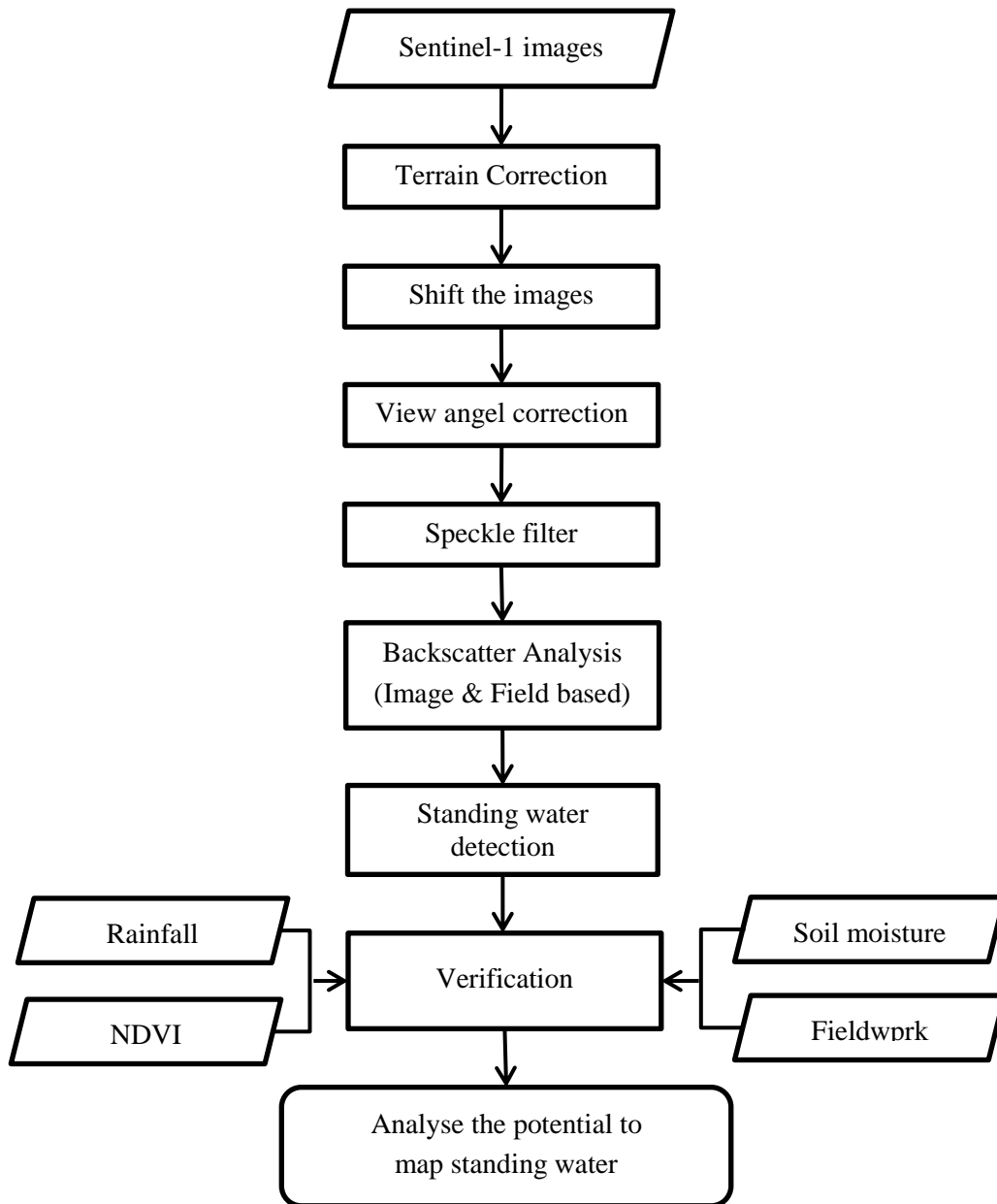


Figure 1 Flowchart of research method

## 2. STUDY AREA AND DATA

### 2.1. Study area

The study area is located in the Twente region in the eastern part of Overijssel province (eastern Netherlands). The study area is between longitudes  $6.6^{\circ}$  -  $7.1^{\circ}$  E and latitudes  $52.1^{\circ}$  -  $51.5^{\circ}$  N, including the city of Enschede as shown in Figure 2. The terrain of the study area is flat, with an elevation ranging between 1 m to 83 m above mean sea level. The land cover of this area includes a mosaic of agricultural fields (winter wheat, corn fields and grassland), forest patches and several urban areas (Dente et al., 2012). The average temperature in Enschede is  $9.1^{\circ}$  C and the average annual rainfall is 782 mm. Monthly precipitation amounts are evenly spread over the year. Monthly precipitation from 1974 to 2009 is around 70 mm (Dente et al., 2011).

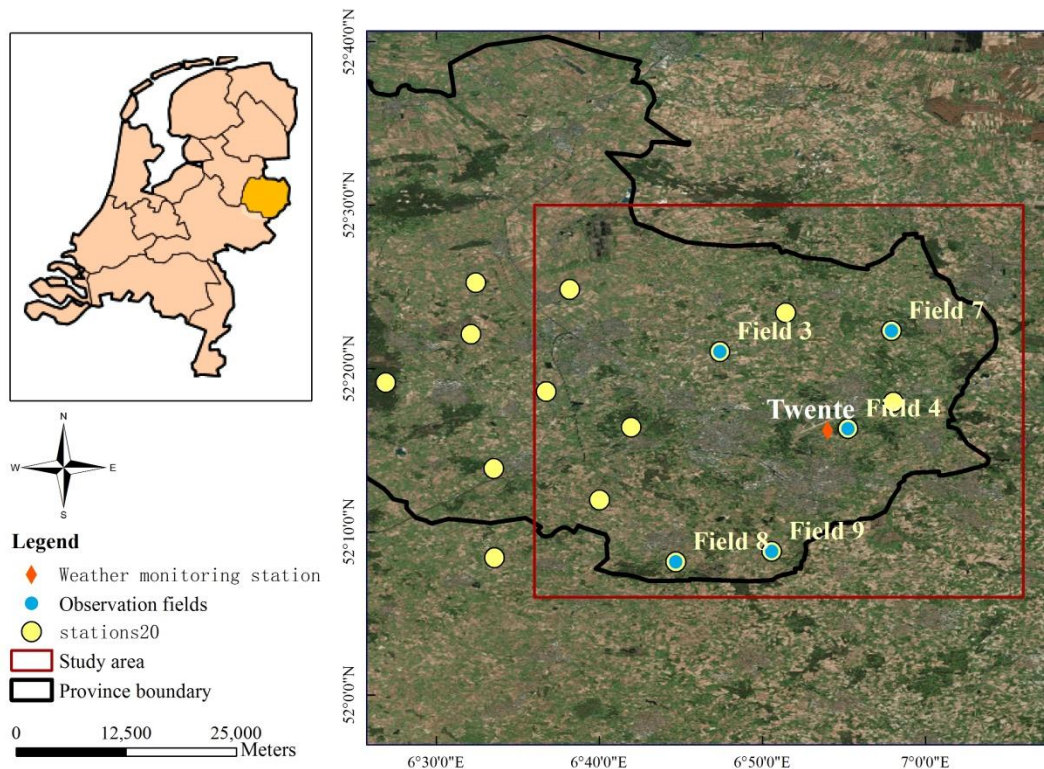


Figure 2 On the left: map of Netherlands with the Twente region highlighted. On the right: Google Earth image of the area covered by the soil moisture stations and weather monitoring stations belong to the Royal Netherlands Meteorological Institute (KNMI).

### 2.2. Sentinel-1 data

In this research, Level-1 Ground Range Detected (GRD) Sentinel-1 C-band (5.405 GHz) data collected in the Interferometric Wide swath (IW) mode were used. This mode allows the combination of a large swath width (250 km) with a moderate geometric resolution (10 m). Moreover, it has dual-polarization capability (HH+HV or VV+VH) which can provide more ground surface information. 73 SAR images have been used for the period from October 2014 to September, 2015, which are freely available from the European Space Agency (ESA) through Sentinels Scientific Data Hub (<https://scihub.esa.int/dhus/>). The time interval of the acquired images varies from 2 days up to 11 days. The main characteristics of the collected Sentinel -1 IW data are provided in Table 1 (Torres et al., 2012). The IW mode is the default acquisition mode over land.

Table 1 Characteristics of the Sentinel-1 Interferometric Wide swath mode nominal measurement modes (Torres et al., 2012; Sentinel-1 Team, 2013).

Parameter	Interferometric Wide-swath mode(IW)
Swath width	250 km
Incidence angle range	29.1 ° - 46.0 °
Sub-swaths	3
Azimuth steering angle	$\pm 0.6$ °
Azimuth and range looks	Single
Polarisation options	Dual VV+VH
Maximum Noise Equivalent Sigma Zero (NESZ)	-22 dB
Radiometric stability	0.5 dB (3 $\sigma$ )
Pixel size (meter)	10

### 2.3. Rainfall data

The daily rainfall data are available from the Royal Netherlands Meteorological Institute (KNMI, <http://www.knmi.nl/nederland-nu/klimatologie/daggegevens>). In this study, daily rainfall data from October, 2014 to September, 2015 were collected at the Twente station located in the Twente region near Enschede (Figure 2). As shown in Figure 3, the rainfall is spread over the study period. It is clear seen that rainfall events concentrated in July and August. The peak of daily rainfall occurs in August as high as 34.2 mm a day.

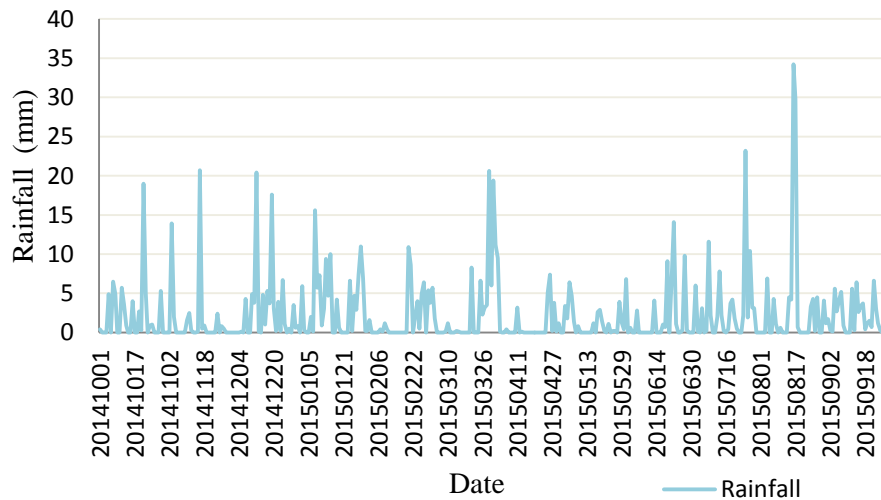


Figure 3 Daily rainfall from 2010 to 2014 in Twente KNMI monitoring station as highlight in Figure 1

### 2.4. Soil moisture data

Soil moisture data are derived from the ITC soil moisture monitoring network (L Dente et al., 2011). There are 20 stations in the soil moisture monitoring network which are located over eastern part of the Overijssel province. All the soil moisture sites are marked as yellow points in Figure 2. The 20 soil moisture stations spread over an area of about 50 km  $\times$  40 km large area (52°05' - 52°27'N, 6°05' - 7°00'E). Soil moisture data has been recorded every 15 minutes, while in some field the data is missing. In each observed field, there is a soil moisture monitoring station. The observed field was named after the number of soil moisture monitoring station in the same field. During the fieldwork, 5 fields named after the soil moisture sites (No. 3, 4, 7, 8, 9) had been visited. The soil moisture measurements are collected at both 5 and 10 cm depth. As Sentinel-1 is to provide C-band SAR data, top layer soil (5 cm) moisture data is used to verify the possible standing water.

## 2.5. Vegetation index

The Normalized Difference Vegetation Index (NDVI) is a numerical indicator for the amount of green biomass with a value between 0 and 1. It has been widely applied to estimate crop yields, pasture performance, and rangeland carrying capacities among others. In this study, MODIS NDVI was utilized first for considering the crop growth stage and agricultural activities. NDVI 16-day interval product (250 m) composite grid data (MOD13Q1) in HDF format were acquired for the period between October 2014 and September 2015 (23 images) from the NASA Earth Observing System (EOS). However, due the observed field is as small as 220 m ×450 m (e.g., No.3 field, the relatively larger one). The MODIS NDVI product is not good enough to describe the vegetation density at such small scale. Therefore, vegetation index (NDVI) was derived from Groenmonitor website (<http://www.groenmonitor.nl/groenindex>).

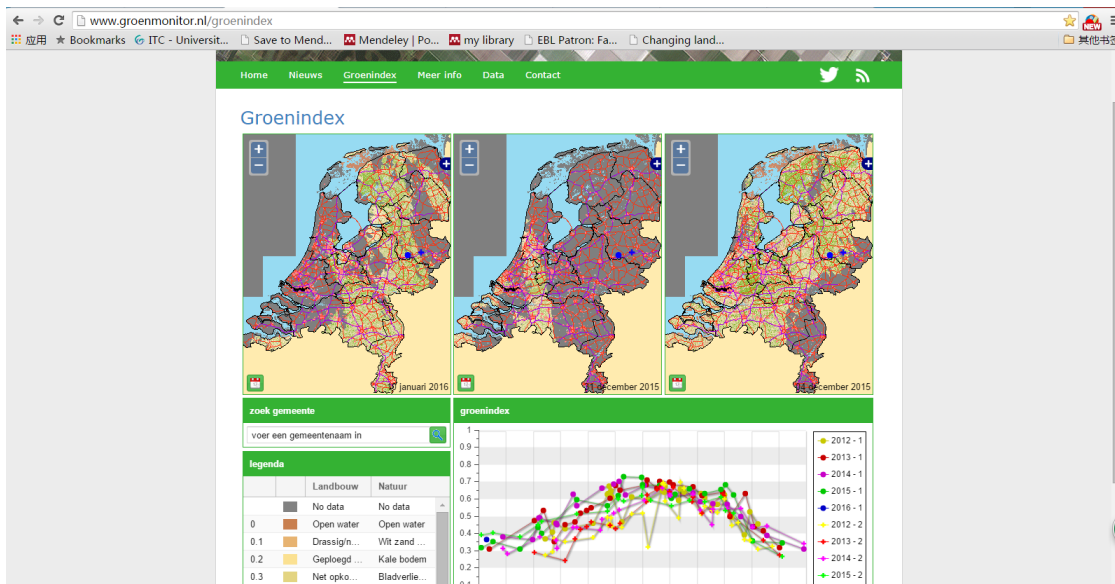


Figure 4 Vegetation Index (NDVI) for observed fields provided by Groenmonitor website (<http://www.groenmonitor.nl/groenindex>)

## 2.6. Land cover data

The land cover map is provided by the Atlas of Overijssel by the Province of Overijssel (<http://gisopenbaar.overijssel.nl/viewer/app/bodematlas/v1>, Figure 5). The main land covers are agricultural fields, forest, and buildings. The main crop is corn, which is seeded in April/early May, and harvested in September/October. Another important seasonal crop is winter wheat. Perennial grassland are used for pasture or harvested several times a year. In this study, the land cover of observation fields includes winter wheat, corn and grassland.

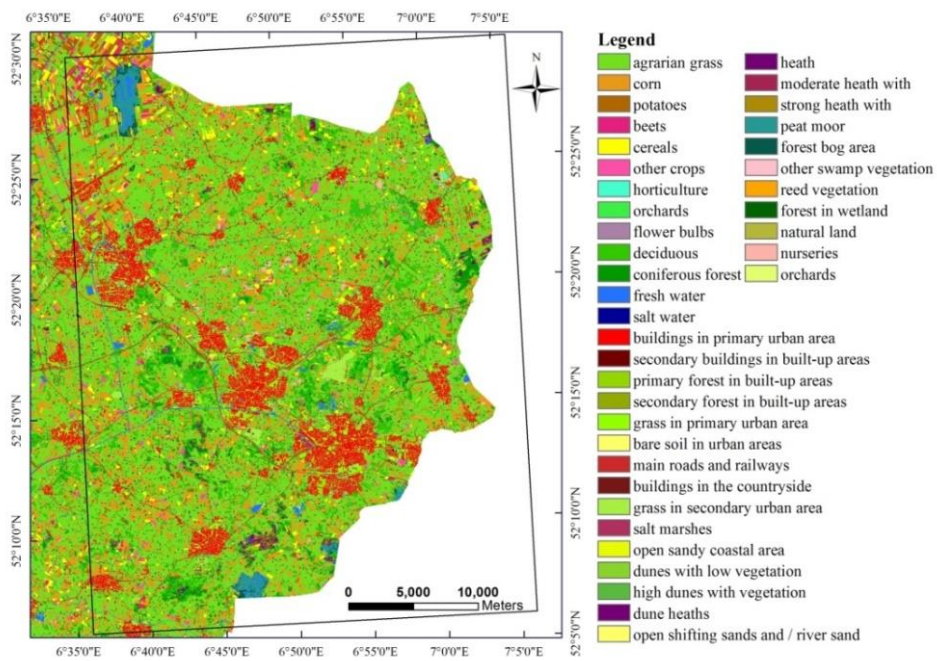


Figure 5 Land cover map of study area available on the website of Overijssel by the Province of Overijssel (<http://gisopenbaar.overijssel.nl/viewer/app/bodematlas/v1>)



### 3. METHODOLOGY

Delineation of standing water from SAR data mainly makes use of the unique characteristics, e.g. water body exhibit in interaction with microwaves. Calm open water acts as a specular reflector, scattering the incoming signal reflects away from the sensor (Figure 6 a). Since the sensor receives a low backscattered signal, water appears dark in the SAR images compared to the backscatter signals from vegetation or other land surfaces. Compared to water, microwaves incident on a rough surface are scattered in many directions, which is known as diffuse reflection and result in a brighter tone on the radar imagery (Figure 6 b). Moreover, backscatter is also affected by the dielectric properties of the surface. When surface water disappeared shortly after the event of standing water, the soil moisture is close to saturation. The increase of the soil dielectric constant with water content leads to an enhanced signal return unless the inundation doesn't over the area when it rained or the surrounding soils were already saturated before the flooding (Hostache et al., 2012). Those backscatter changes can be used to delineate the water logged areas. However, the yearly vegetation cycles may also cause changes of backscatter, such as volumetric scattering from a tree (Figure 6 c). With volume scattering, radar sensor may receive backscatter from both the target surface and the interior volume scattering of the target. Furthermore, some surface objects with respect to dry, bare sand, such as paved highways, may be easily confused with calm open water bodies due to the similar low backscatter from their surfaces.

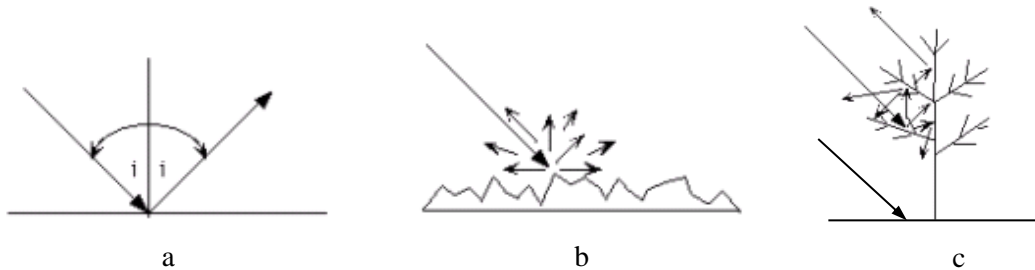


Figure 6 Scattering mechanisms (<http://imaging.geocomm.com/faq/>)

#### 3.1. Fieldwork

Fieldwork has been done from 17<sup>th</sup> September, 2015 to 2<sup>nd</sup> October, 2015, nearly twice a week and in total 5 times. The main purpose of the fieldwork is to find the standing water in agricultural fields and record the outline of the water areas by using GPS. At the same time, the landscape was described in the observation note. Also the time of landscape changes and agricultural activities were recorded in order to analyse backscatter changes with respect to human activities.

#### 3.2. Identification of agricultural areas

As the features of standing water in SAR imagery are the results of different factors, mainly including surface roughness, soil moisture, and vegetation biomass. The characteristics of backscatter are different for different land cover types or different time period for the same field. Therefore, those characteristics of backscatter were expected to contribute to identify the land cover type and delineate the agricultural areas. The cross-polarized information of SAR is known to be sensitive to volume scattering processes and can be related to the land cover type and structure of vegetation (Cloude, 2009). In this study, backscatter temporal variability was calculated from pixel basis dual-polarized information for 73 images. Previous studies indicated that vegetated area backscatter variations are

more stable in densely vegetated, deep-rooted area than in less dense areas, such as grass (Mtamba et al., 2015). In densely vegetated areas, such as forest, the backscatter response is more or less constant during all seasons because they can maintain their water content even during the dry season. Previous literature also showed that the separation between forest and agricultural fields is good based on temporal variability (Figure 7), mainly due to the higher variability effected by the factors mentioned above. Urban areas usually with low temporal variability (Bruzzone et al., 2004). In order to better identify the agricultural areas, the mean backscattering coefficient can be used to increase the effectiveness of feature set consideration.

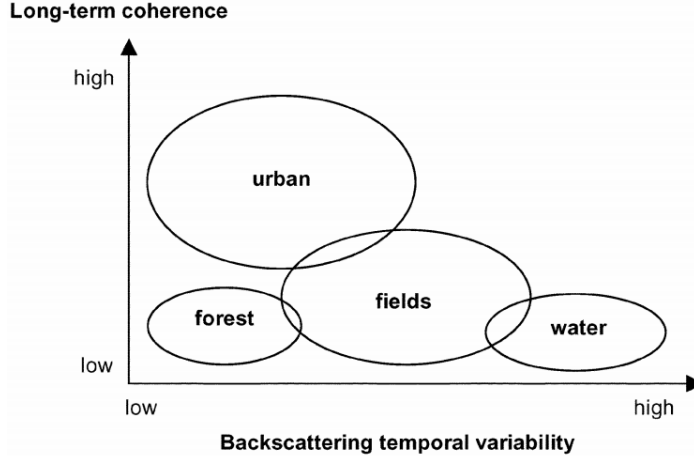


Figure 7 The distribution of land cover classes in the backscatter temporal variability and long-term coherence feature space (Bruzzone et al., 2004).

Previous study showed that high mean backscatter and low standard deviation were observed in forest/papyrus/thicket vegetation areas (Mtamba et al. 2015). Agricultural fields outside the floodplain were characterized by low backscatter and high standard deviation. For the above reasons, backscatter temporal variability estimators relative to the SAR signal feature are used to locate agricultural areas. The land cover map shown in Figure 5 and Google Earth were used to validate results. The estimation of temporal variability from the backscatter can be derived according to the following estimators of N SAR images (Table 2).

Table 2 Backscatter estimators

Estimators	Equations
Standard Deviation	$\text{stdev} = \sqrt{\frac{1}{N} * \sum_{i=1}^N (\sigma_i^2 - \sigma_{\text{ave}}^2)}$
Normalized Standard Deviation	$\frac{\text{stdev}}{\sigma_{\text{ave}}} = \sqrt{\frac{1}{N} * \sum_{i=1}^N \frac{\sigma_i^2}{\sigma_{\text{ave}}^2} - 1}$
Logarithmic Measure Based on Normalized Standard Deviation	$10 * \log_{10} \left( \frac{\text{stdev}}{\sigma_{\text{ave}}} + 1 \right)$
Saturation	$\text{saturation} = \frac{\sigma_{\text{max}} - \sigma_{\text{min}}}{\sigma_{\text{max}}}$
Standard Deviation of dB Values:	$\text{stdev} = \sqrt{\frac{1}{N} * \sum_{i=1}^N (10 * \log_{10} \sigma_i)^2 - \left( \frac{1}{N} * \sum_{i=1}^N 10 * \log_{10} \sigma_i \right)^2}$
Maximum-Minimum Ratio in dB	$10 * \log_{10} \left( \frac{\sigma_{\text{max}}}{\sigma_{\text{min}}} \right)$

Those estimators are mentioned in the study of Bruzzone et al. (2004). Where  $\sigma_{max}$ ,  $\sigma_{min}$ , and  $\sigma_{ave}$  are the maximum, minimum and mean backscatter values of the M intensity SAR images,  $\sigma_i$  is the backscatter coefficient of image  $i$ . The standard deviation (*stdev*) is a measure that is used to quantify the amount of variation or dispersion of a set of data values. The value of standard deviation closing to 0 indicates that the data points tend to be very close to the mean value of the set, while a high standard deviation indicates that the data points are spread out over a wider range of values. The Normalized Standard Deviation is a process that mapping the data to a range of 0 to 1. Those two estimated values are more convenient and fast for application. Besides, the normalized standard deviation estimator also converts the dimensional expression to dimensionless expression. Saturation measures the relative range of the backscatter values over a series of images. So when the saturation is large then there is a large difference between the maximum and minimum backscatter, relative to the maximum backscatter. When the saturation is small the maximum and minimum backscatter are relatively close to each other. Out of the six estimators, Bruzzone et al. (2004) chose the standard deviation of decibels values to derive the backscattering temporal variability characteristics. In this study, the estimators in the Table 2 were tested to get the backscatter temporal variability, and 73 images were used to calculate temporal variability on pixel basis using IDL.

### 3.3. Standing water detection and verification

Within the study area, the observed fields are far away from a river, therefore fluvial flooding is not likely to occur. Standing water is generated either by rainfall failing to infiltrate because of low infiltration capacity or by rainfall falling on to already saturated ground. Smooth surface causes specular reflection, thus open water results low backscatter observations in SAR images. So in the SAR image, the relatively low values of backscatter would be probably due to the periodically standing water. However, the smoothness of surface is also determined by other factors, such as soil surface roughness, vegetation biomass. As backscatter in SAR image are the result of different factors, including acquisition characteristics (wavelength, incidence angle, polarization), soil moisture, vegetation characteristics, and soil surface conditions (roughness and standing water). The relatively low backscatter, on the other hand, would not just because of the standing water. Low backscatter would occur as a result of low soil moisture, smooth surface without vegetation covers or standing water in the fields. Hence, in this study the possible standing water was verified via ancillary data, including soil moisture, in-situ rainfall, and NDVI.

A polygon was made for each observed field, which was used to extract the backscatter coefficient for the study period. Those regions of interesting were created in the centre of the field in order to avoid the interference of the field boundary effect, such as tree canopy. Also, the signal of each observed field will be approximated by averaging calculation in order to decrease the effects of speckle. For this part, the goal is to study the backscatter variation with the trend of rainfall, soil moisture and NDVI changes. For that purpose, all possible relevant factors were plotted and analysed with low values of VV- polarized backscatter change.

## 4. FIELDWORK

### 4.1. Description of the observed fields

Figure 8 shows the landscape of all the visited fields in September. Each observation field was named by the soil moisture station name installed in the field as highlight in blue point in Figure 2. No.3 and No.4 field are grassland for the pasture. The grass in both fields is about 60 cm high before harvest. No.4 grassland has the higher elevation among all the observed fields which is between 45 m to 50 m. Surface water under the grass spreading as mosaic in the No.4 field. No.7 field contains three fields with elevation about 23 m. Two of them are winter wheat fields that had obviously surface ponding, and the other one is corn field. The area of No.7 winter wheat field is 42247 m<sup>2</sup> for the left and the 60733 m<sup>2</sup> for the right side field. Winter wheat in the No.7 field had already been harvested before 17<sup>th</sup> September, while wheat-straw was left in the field mixing with the grass. Compared to No.9 winter wheat field, surface condition of No.7 winter wheat field is more complex. Standing water spread randomly in the lower places, like footprints left by the harvester. The standing water area was randomly spread and the largest one was 10 m × 5 m. No.8 is also mature corn field. The corn in the observed field was quit thick about 2 meters high. Land cover of No.9 belongs to winter wheat. The surface of No.9 field is quite smooth without too much straw and grass on it.

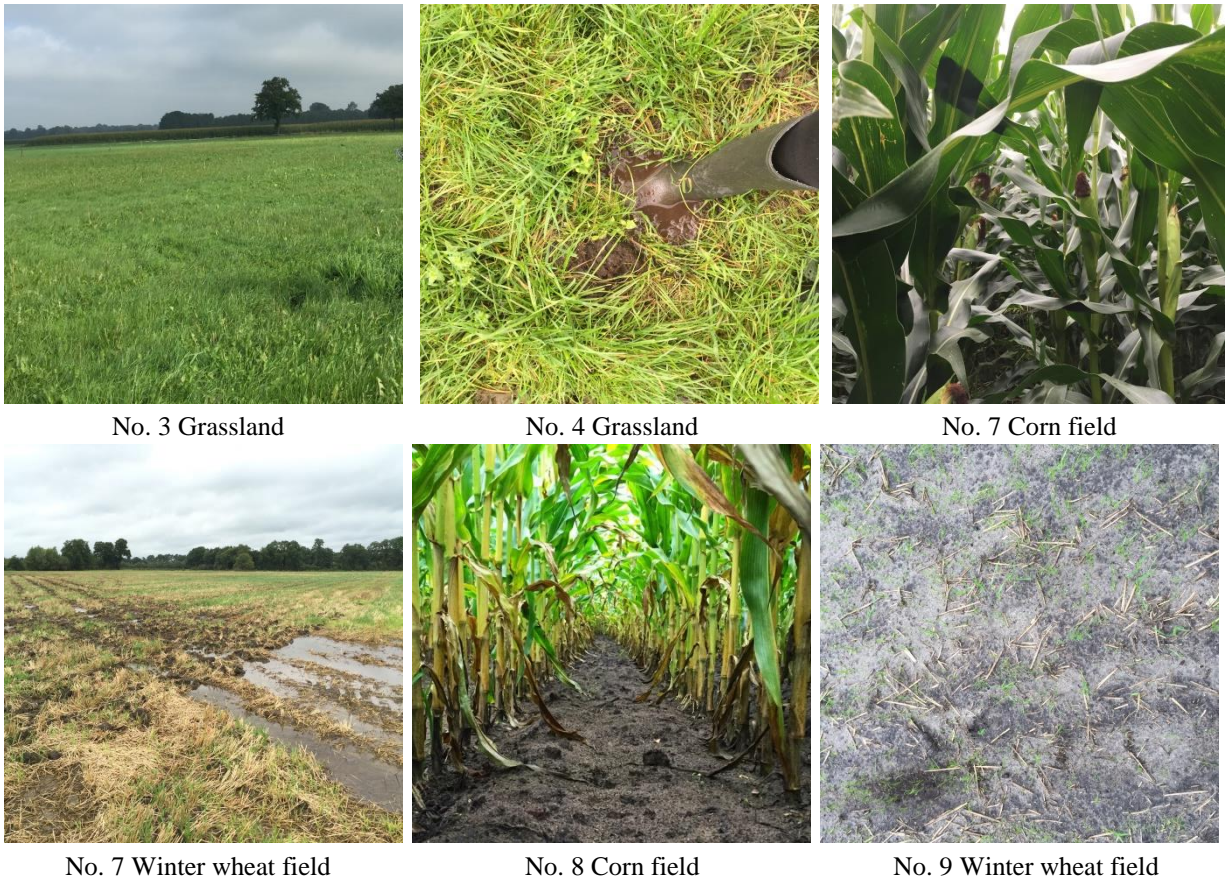


Figure 8 Landscape in each observation field.

### 4.2. Landscape changes during the fieldwork

During the fieldwork period, the landscape of No. 7 field changed quite a lot as shown in Landscape of mature corn in No.7 and No.8 field didn't change. On 30<sup>th</sup> September, the grass in No.3 field had

already been cut. On the same day, the owner of No.4 just started to cut the grass and left it on the ground to be dry. Landscape change of grassland is shown in Table 4 and Table5.

Table 3. In September, the winter wheat had already been cut, while the straws (20 – 40 cm high) were left mixing with grass. On 16<sup>th</sup> September, there was a persistent rain for nearly the whole day. On 17<sup>th</sup> September morning there was ponding water randomly spread over the fields. The standing water area pattern is similar to the trails made by the machine wheels. On 24<sup>th</sup> September, farmers have to dig channels to help surface water drain away. The channels are about 10 to 15 cm deep. On 25<sup>th</sup> September, the weather is clear, but there was still some water in the fields. At the beginning of the October, the farmers began to plough the fields and spread fertilizer. So, there was no obviously water and grass in this field. Landscape of mature corn in No.7 and No.8 field didn't change. On 30<sup>th</sup> September, the grass in No.3 field had already been cut. On the same day, the owner of No.4 just started to cut the grass and left it on the ground to be dry. Landscape change of grassland is shown in Table 4 and Table5.

Table 3 Landscape changes in No.7 observed fields.

No. 07 field	Description
 <p data-bbox="584 1173 708 1205">17-09-2015</p>	<p data-bbox="951 853 1267 884">Weather: Cloudy and shower</p> <p data-bbox="951 927 1305 1173">Description: There was a sustained rainfall on 16<sup>th</sup> September. Water in the fields could cover the instep. Wheat-straw were left mixing with grass. The straw is 20 to 40 cm high above the ground.</p>
 <p data-bbox="584 1565 708 1597">24-09-2015</p>	<p data-bbox="951 1296 1171 1328">Weather: Cloudy.</p> <p data-bbox="951 1370 1305 1509">Description: The farmers have to dig drainage to discharge the surface water. They said the soil type is clay.</p>
 <p data-bbox="584 1933 708 1964">25-09-2015</p>	<p data-bbox="951 1691 1145 1722">Weather: Sunny</p> <p data-bbox="951 1765 1305 1868">Description: There are some grass, wheat-straw, and still some water in the fields.</p>

 <p style="text-align: center;">30-09-2015</p>	<p>Weather: Clear, Sunny</p> <p>Description: farmers begin to plough the field with the fertilizer. There is few grass left in the fields.</p>
 <p style="text-align: center;">02-10-2015</p>	<p>Weather: Clear, Sunny</p> <p>Description: No water and even the grass in the fields. The farmer using the machine to plough the fields.</p>

Table 4 Landscape changes in No.4 observed fields.

No. 04 field	Description
 <p style="text-align: center;">25-09-2015</p>	<p>Weather: Sunny</p> <p>Description: The grass in this area is about 50 cm to 60 cm high and wet. When walk across the grass, it will wet you clothes. Moreover, the grass is density and look smooths on the top</p>
 <p style="text-align: center;">30-09-2015</p>	<p>Weather: Clear, Sunny</p> <p>Description: the owner began to cut the grass and spread them on the ground to be dry.</p>

 <p>02-10-2015</p>	<p>Weather: Clear, Sunny</p> <p>Description: The grass was gone and ground is getting dry.</p>
---	--

Table 5 Landscape changes in No.3 observed fields.

No. 03 field	Description
 <p>25-09-2015</p>	<p>Weather: Sunny</p> <p>Description: The grass in this area is about 50 cm to 60 cm high and wet similar as No.4 field. But a litter bit dry than No.4 grassland. Moreover, the grass is also density and look smooths on the top</p>
 <p>30-09-2015</p>	<p>Weather: Clear, Sunny</p> <p>Description: The grass has been harvested and gathered. The stems left in the field are 10 cm to 15 cm high.</p>
 <p>02-10-2015</p>	<p>Weather: Clear, Sunny</p> <p>Description: The dry grass was packed as the white boxes. The grass left in the ground was about 10 cm to 15 cm high.</p>

## 5. SENTINEL-1 DATA PRE-PROCESSING

SNAP software (Sentinels Application Platform, <http://step.esa.int/main/download/>), particularly the S-1 Tool box of the SNAP was utilized to pre-process the SAR imagery. SAR data can be accessed by targeting the entire Sentinel ZIP file in SNAP. The original SAR image is inverted in the SNAP. It is displayed according to the order of data acquisition, which is not according to a cartographic representation. To reproject the images from geometry of the sensor to the geographic projection, terrain correction was applied. The influence of the incident angle on the received signal is significant (G. J.-P. Schumann & Moller, 2015). Particularly in the modes of sensor operation that use the full swath of the orbit track (O’Grady et al., 2013). Therefore, an incidence angle correction is needed. Furthermore, the synthetic method used for creating the SAR imagery also has some disadvantages. Inherent to the measurement technique is random constructive and destructive interference of waves will cause the SAR images to be noisy. This noise within the SAR images is called speckle and decreases the quality of the image and making interpretation of features more difficult. A number of speckle filter types are provided in SNAP. Speckle noise reduction was applied by using single product speckle filter. Different filter types were simply test by visually comparing the filter results.

Therefore, the data processing including terrain correction, subset, speckle filter, shift by the ground control points, incidence view angle correction, and convert from intensity ( $m^2 m^{-2}$ ) to decibel (dB). The flowchart for data pre-processing is shown below.

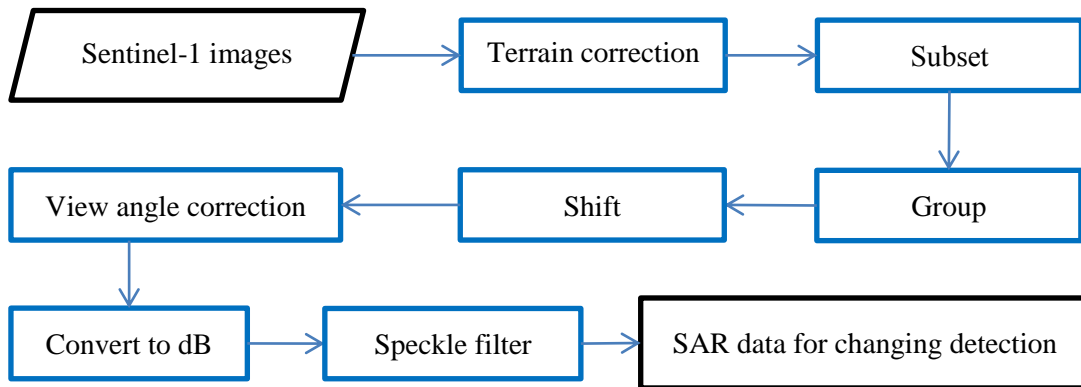


Figure 9 Sentinel-1 data processing steps

### 5.1. Terrain correction

Upon completion of the terrain processing a file is created with 3 bands called ‘sigma0\_HH’, ‘sigma0\_VH’ and ‘ProjectedIncidenceAngle’. The ‘sigma0\_VV’ and ‘sigma0\_VH’ bands include the backscattered cross section in intensity units ( $m^2 m^{-2}$ ). The exploration of the ‘ProjectedIncidenceAngle’ band shows that the incidence angle is expressed in degree.

After Range Doppler Terrain Correction, using bilinear interpolation and SRTM 3sec as Digital Elevation Model (DEM), there was a shift in longitude of about 9 pixels for the different image passes (ascending / descending). Other available DEMs in the SNAP tool-box were tested, such as SRTM 1sec, ACE30, but the shift remains. Therefore, ground control points (GCP) were used to georeference the shifted data. First of all, data were grouped by its ascending and descending passes properties, which can be found in the Metadata. The cross points of the road in SAR images were selected as GCPs and then the images are shifted by IDL.

## 5.2. View angle review

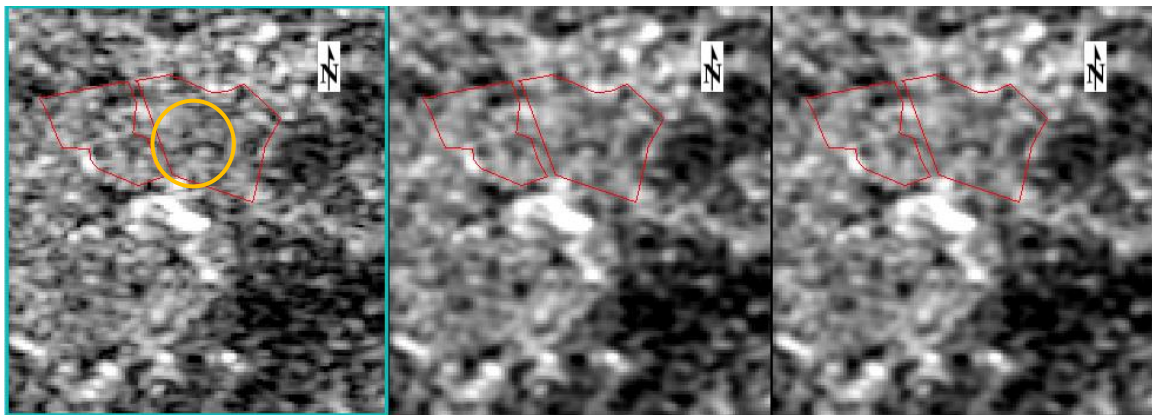
Sentinel 1 satellite data are collected at view angle ranging from 29.1° to 46.0°. Incidence angle describes the angular deviation of the incident signal from nadir. Correction for  $\sigma^0$  differences due to this angular variability is needed. This is often done by normalizing the observations towards a reference angle. Besides, the backscatter is dependent on the incidence angle, so to limit the effect of the incidence angle the backscatter normalization is needed. The most commonly adopted method is the cosine correction (Mladenova et al., 2012) whereby the  $\sigma^0$  is normalized towards a reference angle using,

$$\sigma_{ref}^0 = \sigma^0 \frac{\cos^n(\theta_{ref})}{\cos^n(\theta_v)} \quad \text{Equation 1}$$

Where  $\theta_v$  is the incidence view angle (degrees),  $\sigma_{ref}^0$  is the normalized backscatter based on a reference angle,  $\theta_{ref}$  ( $m^2 m^{-2}$ ), and  $n$  depends on the type of scattering and ultimately the land cover characteristics (-) (Velde et al., 2014). In some soil moisture retrieval methods (i.e. Change Detection techniques) the reference view is often defined as 30 degrees (Dostálová et al., 2014). When reradiation of the incident energy follows the cosine law, instead of being isotropic,  $n$  should be taken equal to 1, which is in essence an application of Lambert's law for optics (Velde et al., 2014). This process was implemented in IDL.

## 5.3. Speckle filter

Speckle filtering is needed to suppress the noise in order to allow better interpretation and backscatter analysis. However, speckle filters not only suppress the noise, but also remove observations that are not affected by noise and contain valuable land surface information (e.g. soil moisture, biomass and flood extent). Here, single product speckle filter method in SNAP was used to remove the speckle. The SNAP S1 Tool box operator supports the following speckle filter types for handling speckle noise of different distributions (Gaussian, multiplicative or Gamma): Mean, Median, Lee, Refined Lee, and Gamma-MA. Because of the fact that standing water in the observation fields is only 10 m × 5 m while the pixel size of Sentinel-1 image is 10 m. The window size was defined as 3 × 3. Figure 10 displays the test result of different filters with same size of moving filter windows on Sentinel-1 image acquired in 16<sup>th</sup> September, 2015. Those images illustrate standing water in the No.7 winter wheat field. According to Figure 10, the Refined Lee filter shows more clear standing water boundary as highlight in the orange cycle. Because of the standing water area is relatively small compared to the pixel size of the SAR observations resolution. Refined Lee filter was applied because it maintains the detail of the standing boundary.



Refine Lee

Lee

Gamma Map

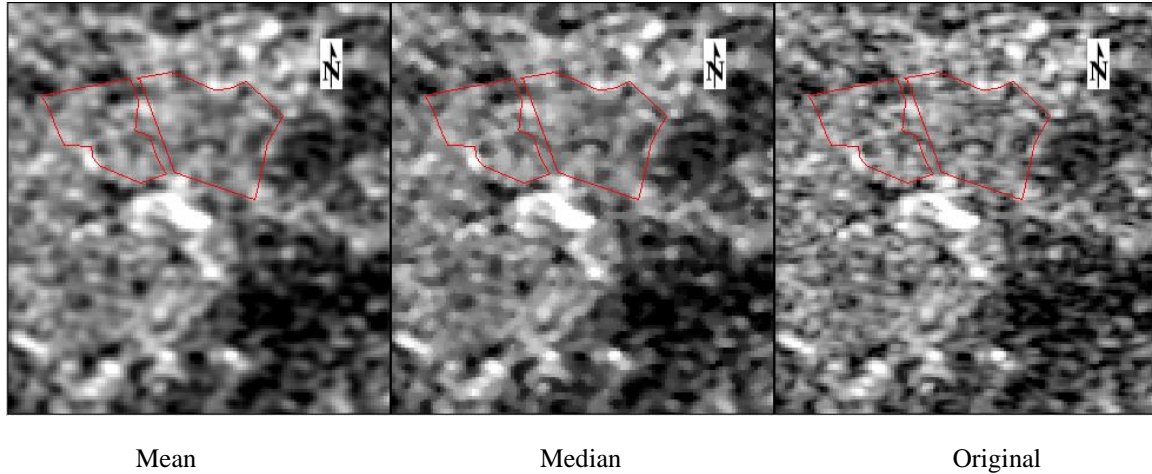
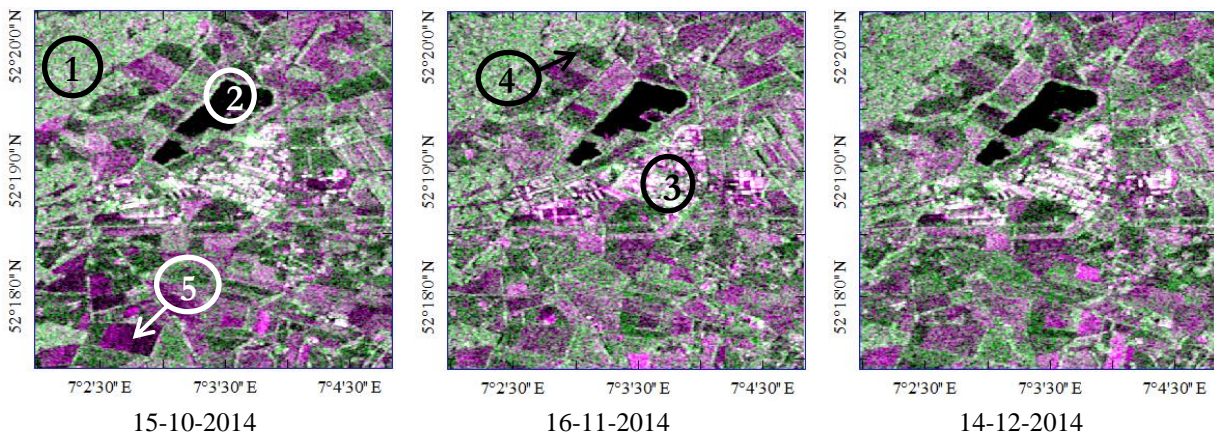


Figure 10 Filter results of VH-polarized SAR images acquired on 16-09-2015

An RGB colour composite for visually interpretation (Red and Blue – VV polarization; Green – VH polarization) was made (Figure 11) for visual interpretation of landscape changes. Combining with fieldwork observation, it can be observed that the light greenish colour (Figure 11 15-10-2014 ①) represents the differences between VV and VH backscatter signal, which indicated the presence of density vegetation, such as forest. The dark greenish colour (Figure 11 16-11-2014 ④) refers to the grassland, related to its smooth surface. The light purplish colour (Figure 11 16-11-2014 ③) refers to built-up areas, such as houses. The black areas (Figure 11 15-10-2014 ②) stands for low VV and VH backscatter signals, related to smooth surface, usually open water bodies and bare soil (Twente Airport). However, it was also observed that corn fields and winter wheat fields (Figure 11 15-10-2014 ⑤) are looks similar, which in purplish. From the visual interpretation for vegetated areas of these SAR processed images, backscatter of forest is relatively constant during the study period from October 2014 to September 2015. The backscatter variation in forest is more stable over the year than the grassland and agricultural fields (corn, winter wheat, grassland). For grassland, the RGB composite colour doesn't change frequently throughout the period. This indicates that grass is more constant. However, the RGB colour of winter wheat and corn field as show in Figure 11 ⑤ changes quite often which is probably due to its vegetation growth, surface conditions changes.



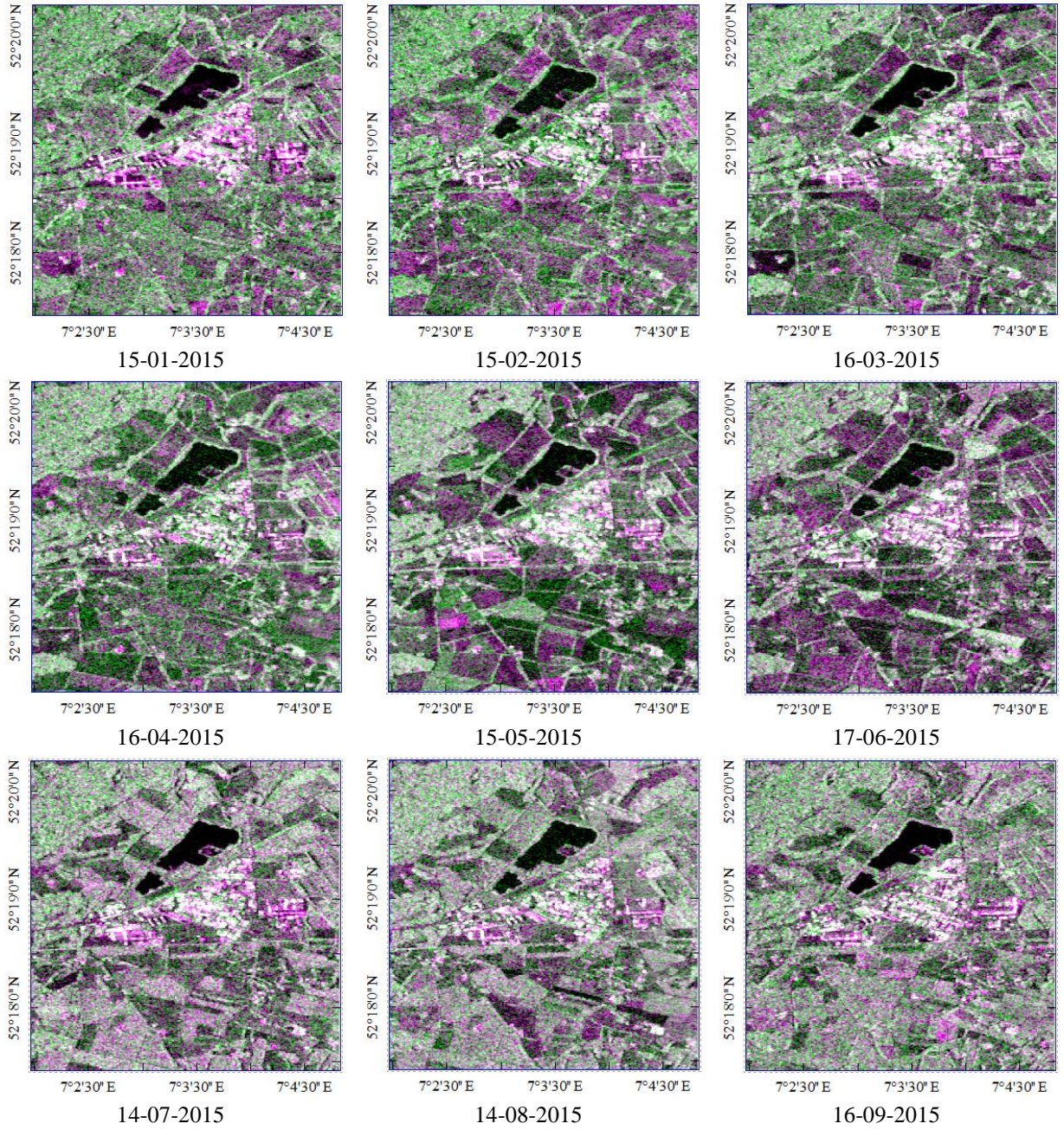


Figure 11 Backscatter (in dB) for RGB colour composite (Green--VH polarization; Red and Blue--VV polarization) at different dates.

## 6. BACKSCATTER ANALYSIS

### 6.1. Image based backscatter analysis

Based on the previous study, estimators for backscatter temporal variability were tested in this area. The other calculated results are displayed in Figure 12 with RGB colour composite (Green--VH polarization; Red and Blue--VV polarization) for visual interpretation. According to the Figure 12(a,b), saturation map and Maximum minus minimum ratio map do not provide a clear characteristics of backscatter for land cover classification. Combining with the land cover map shown in Figure 5, it can be seen that the purplish colour shown in the Figure 12(c) refers to the urban area and the white color in Figure 12 (d) indicates the smooth surface targets, like airport and open water body.

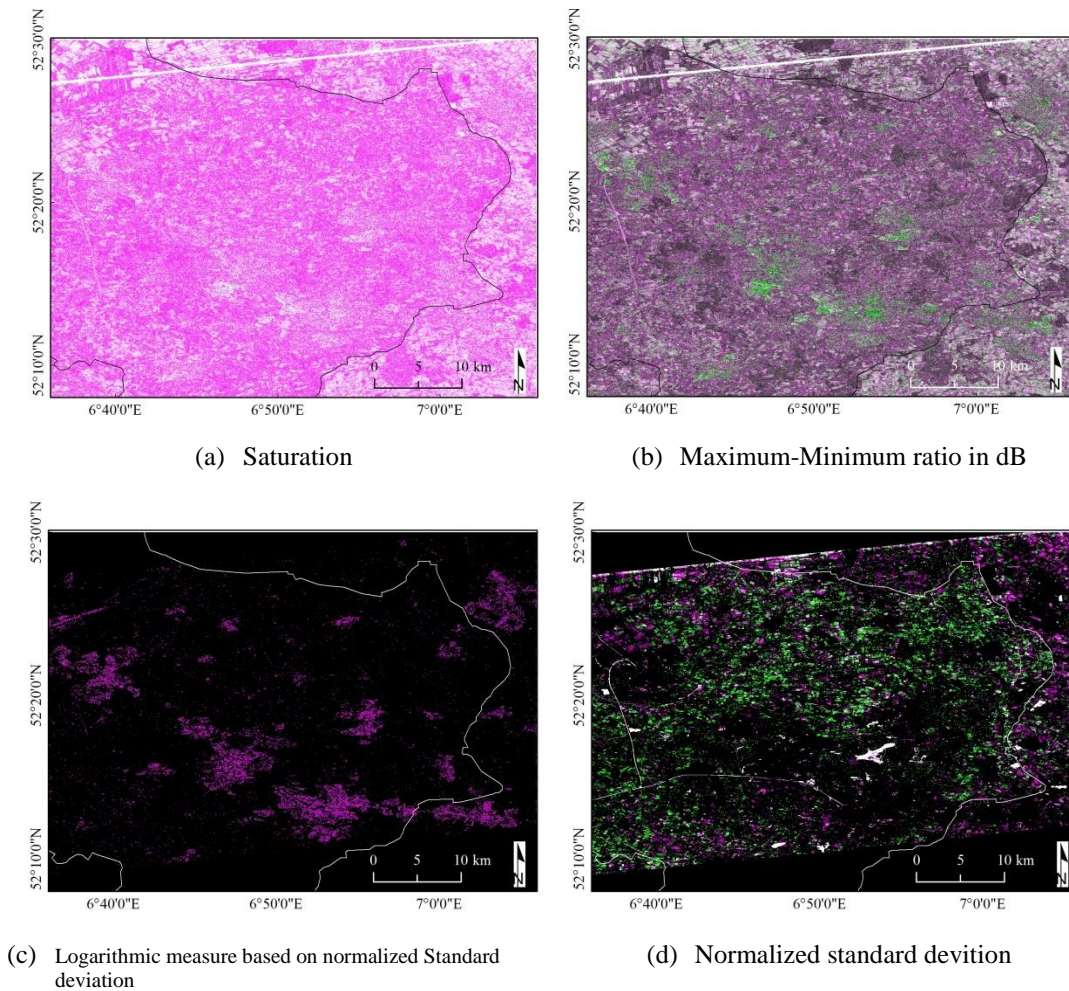


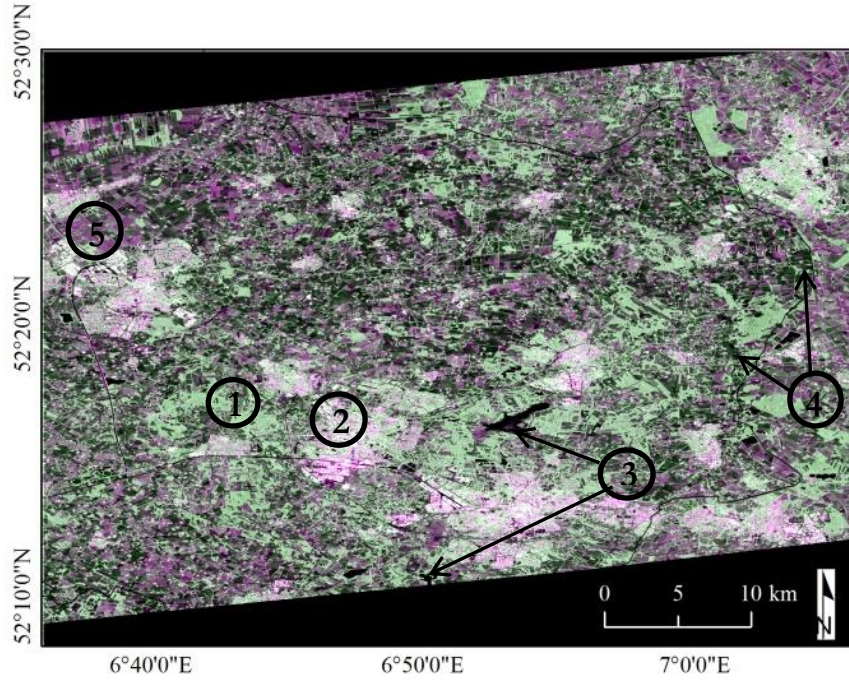
Figure 12 Backscatter temporal variability calculated by different estimators for RGB colour composite (Green--VH polarization; Red and Blue--VV polarization) at different dates : (a) Saturation backscatter; (b) Maximum-Minimum Ratio in dB; (c) Logarithmic measure based on normalized Standard deviation; (d) Normalized standard deviation

Compared to the above 4 estimators, standard deviation of dB values and mean backscatter show the relatively better distinguish for most land cover classification. Therefore, in this research, standard deviation of dB Values (Equation 2) and mean VV and VH polarized backscatter were calculated to analyse the temporal backscatter variability.

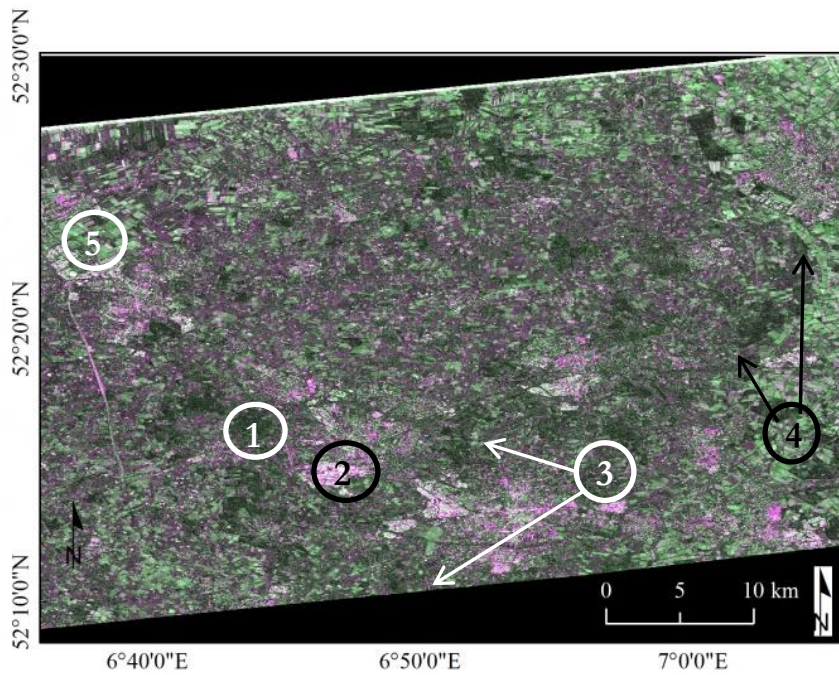
Standard Deviation of dB Values:

$$\text{stdev} = \sqrt{\frac{1}{N} * \sum_{i=1}^N (10 * \log_{10} \sigma_i)^2 - \left( \frac{1}{N} * \sum_{i=1}^N 10 * \log_{10} \sigma_i \right)^2} \quad \text{Equation 2}$$

where  $\sigma_i$  is the backscatter coefficient of image  $i$ . There are  $N$  images in total.



(a) Mean backscatter (in dB)

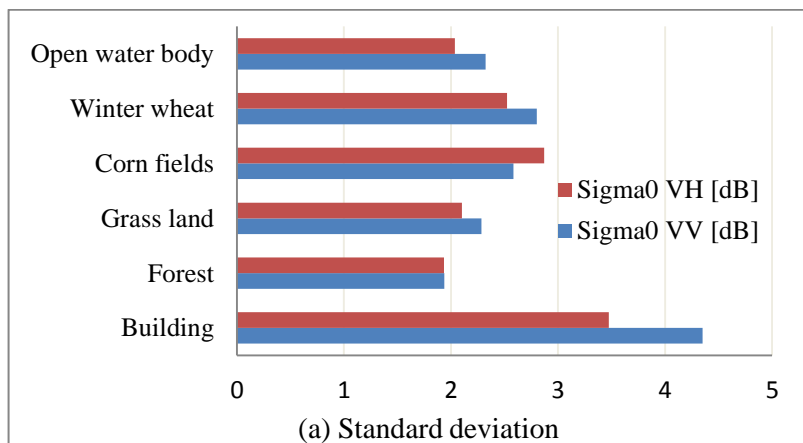


(b) Standard deviation of backscatter (in dB)

Figure 13 Backscatter statistics result for RGB colour composite (Green--VH polarization; Red and Blue--VV polarization): (a) mean backscatter (in dB); (b) standard deviation of backscatter (in dB)

Figure 13 shows an RGB colour composite (Red and Blue – VV polarization; Green – VH polarization) was made from average backscatter statistic image and standard deviation (stdev) map of VH and VV-polarized backscatter for visual interpretation. Combining with fieldwork observation, it can be observed from the mean backscatter map (Figure 13 a) that the greenish color (Figure 13 a ①) indicates the presence of forest. While in the stdev map (Figure 13 b) forest is in a dark tone because they are much more stable not changed much by the rainfall and its growth stage. The bright purplish colour in the Figure 13(a ②) refers to the urban areas. Although urban is the most stable land cover compared to others, urban shows a light colour in stdev map due to surface building material, trees canopy effect, and noisy. The black areas in Figure 13 (a ③) stands for low VV and VH backscatter signals which belongs to open water bodies, roads and bare soil (Twente Airport). However, open water body is not very outstanding in the *stdev* map. For agricultural fields, the dark greenish color in Figure 13(a ④) represent the grassland, related to densely leaves and smooth surface. However, the corn fields and winter wheat fields have a similar colour (purplish Figure 13 a ⑤) in average backscatter image. While in stdev map, crop field are more markble which in the greenish colour. Possible reason for the different colour in those two map may be due to the landscape seasonal change from roughness bare soil to the densely crop covers.

Based on the backscatter statistic results, temporal variation of backscatter and mean backscatter for different land cover were extracted by zonal statistics in ENVI software. According to the Figure 14, open water body has the lowest backscatter due to the specular reflection over the smooth water surface, and similar standard deviation as grassland. This is possibly due to waves on the water surface caused by the wind and the aquatic plant. Temporal variability of forest is the lowest while forest has higher average backscatter because its typically constant over time and less affected by the surface conditions. Relatively higher standard deviation is found in agricultural field, including corn fields and winter wheat. Because of the seasonality of agricultural activity, soil moisture changes and weather conditions, corn fields and winter wheat fields have higher standard deviation compared to the grassland.



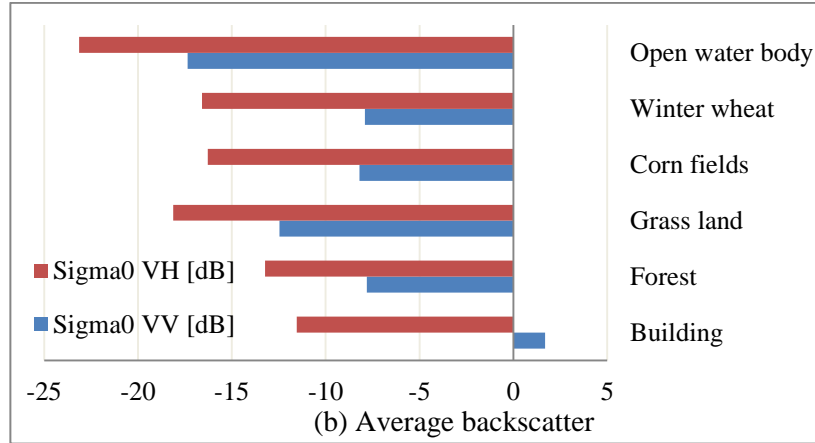


Figure 14 Backscatter statistics for different land cover classes, (a) Standard deviation for VH and VV polarization, (b) Average backscatter for VH and VV polarization.

According to Figure 13 and Figure 14, in this study area backscatter temporal variability derived from SAR imagery (C-band) could contribute to classify the land cover types, like forest, urban, open water body, grassland and agricultural fields. However the temporal variability of backscatter differences between the corn fields and winter wheat field are not obviously enough to distinguish the two crop types from the Sentinel-1 images.

## 6.2. Field-scale backscatter changes and standing water detection

The VV- and VH- polarized backscatter of grassland, winter wheat fields, corn fields, forest and open water body are plotted in Figure 15. The backscatter of each observed field was extracted from the created polygon which is located in the central of the field. In this way, speckle effect can be reduced by average mathematical calculation. Compared to the VH-polarized backscatter, the VV-polarized backscatter has obvious low values and wider obvious fluctuation, which is because of the surface scattering effects give a higher signal on the VV channel. Therefore, in this study VV-polarized backscatter was selected to detection the possible periodically standing water for its evident change.

Table 6 Dynamic range of backscatter in different land cover

	Mean		Maximum		Minimum		Difference	
	$\sigma$ VH [dB]	$\sigma$ VV [dB]						
Wheat No.7 left	-17.14	-8.52	-12.77	-4.70	-21.15	-15.16	8.38	10.46
Wheat No.7 right	-16.78	-8.15	-11.39	-4.27	-21.60	-13.67	10.22	9.40
Wheat No.9 North	-19.27	-10.34	-10.14	-3.28	-25.02	-17.56	14.88	14.28
Wheat No.9 South	-19.00	-10.47	-8.95	-4.61	-25.59	-17.25	16.64	12.64
Corn No.7	-16.42	-8.03	-13.45	-4.20	-20.59	-11.51	7.15	7.31
Corn No.8	-17.79	-9.86	-11.64	-5.24	-22.55	-14.47	10.91	9.23
Grass No.3	-18.06	-12.24	-15.33	-9.56	-20.55	-16.05	5.22	6.49
Grass No.4	-17.81	-11.90	-14.99	-8.96	-20.45	-15.92	5.46	6.96
Water	-24.13	-18.44	-19.887	-12.63	-29.24	-24.27	9.75	11.65
Forest	-13.10	-7.50	-8.65	-3.06	-18.19	-12.54	9.53	9.48

According to Figure 15, backscatter of winter wheat fields has the largest dynamic changes. There are sharply changes around the 16<sup>th</sup> March and 12<sup>th</sup> September. Compared to winter wheat and corn fields, backscatter of grassland is more constant throughout the study period. Dynamic range of backscatter

change of different land cover is shown in Table 6. Grassland has the minor fluctuation and the dynamic range is 6.49 dB and 6.96 dB for VV- polarization in each observed field No.3 and No.4. High fluctuation is found in No.9 winter wheat field varying from -17.56 dB to -3.28 dB. While the fluctuation range in No.7 winter wheat fields is between -15.16 dB to -4.70 dB for left land and -13.67 dB to -4.26 dB for right part. The range difference of backscatter of corn field No.7 and No.8 is 7.31 dB and 9.23 dB, respectively. It also can be seen from the Figure 15 that backscatter changes varies from different land cover types and different location fields with the effect of surface conditions, atmospheric forcings and vegetation characteristics.

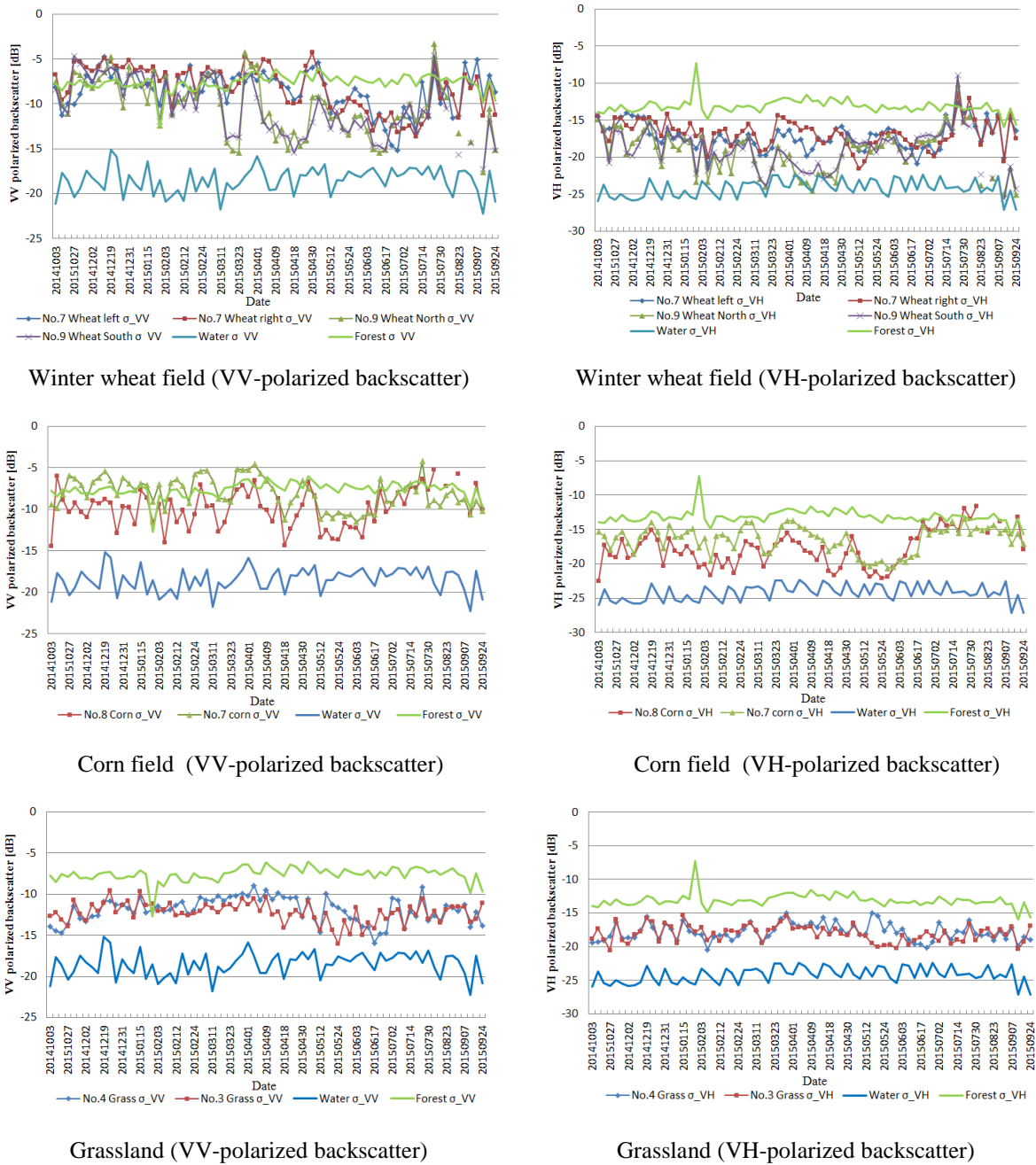


Figure 15 Backscatter changes of different land cover

As described in the section 6.1, open water has the lowest backscatter due to its smooth surface. Forest has higher average backscatter because its typically contant over time and less affected by the surface conditions. Here, backscatter changes of forest and open water body are plotted as the thresholding for

detecting the possible periodically standing water. It is expected that the low backscatter in each agricultural field which is close to the open water body backscatter may be probably because of the standing water. However, changes in land surface conditions (e.g. soil moisture, vegetation biomass) due to atmospheric forcings, and human activities, like ploughing, seeding, and harvesting, affect the backscatter signal observed by Sentinel-1. In the next section, possible periodically standing water was verified with considering effect of the in-situ rainfall, soil moisture, and vegetation biomass.

### 6.3. Temporal verification

In this section, possible periodically standing water was verified using different ancillary data sets such as the in-situ rainfall, soil moisture, and vegetation biomass (NDVI). In-situ rainfall pattern, soil moisture pattern of the whole study area and vegetation biomass of each observed field are first described in 6.3.1 and 6.3.2. Among all the observed fields, No.7 winter wheat field had the obvious surfacing water in the field mixing the wheat-straw and grass in September. While wider fluctuation was found in No.9 winter wheat field. The soil moisture station is built in the right side of No.7 wheat field and north part of No.9 filed. However, some soil moisture measurement data of No.7 station is missing. In order to better verify the possible standing water area here we chose No.9 north part winter wheat field and No.4 grassland as test examples to verify the periodically standing water. The verification of possible periodically standing water will be discussed in section 6.3.3 and 6.3.4 considering with ancillary data.

#### 6.3.1. Rainfall and soil moisture trend

Figure 16 shows the daily rainfall of Twente station from October 2014 to September 2015. According to Figure 16, rainfall nearly spread out the study period with several rainfall peaks and very intensive rain events. There are two rainfall peaks in July and August, where the daily rainfall is more than 25 mm. The accumulation precipitation is 821.8 mm. As the observed fields are far away from river, the main source of water is from rainfall. Therefore, standing water is generated either by rainfall failing to infiltration because of low infiltration capacity or by precipitation falling on to already saturation ground. It also can be seen that soil moisture averaged from all 20 stations is in a good agreement with the rainfall pattern. From December to June, there is an obvious increasing trend of soil moisture with increasing rainfall or intensive rainfall events. However, the fluctuation of soil moisture is not very significantly in the July and August as there was two rainfall peaks.

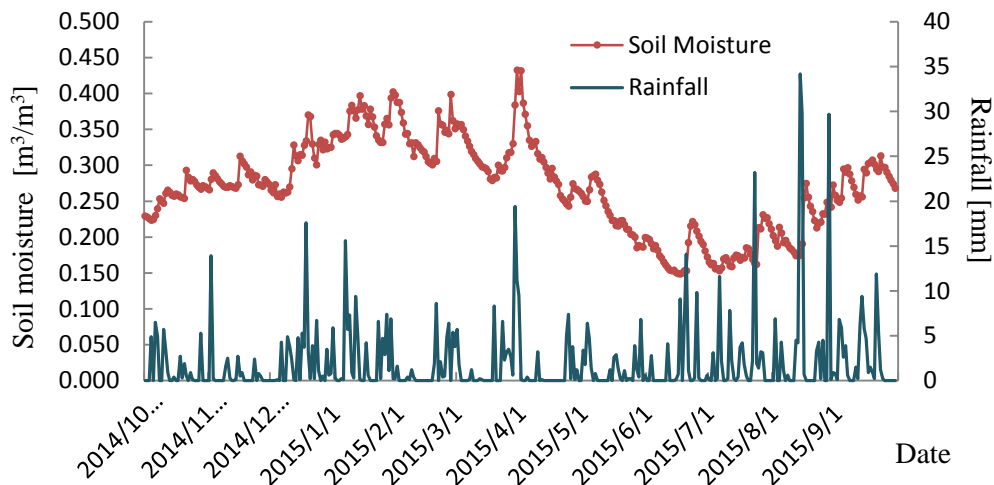
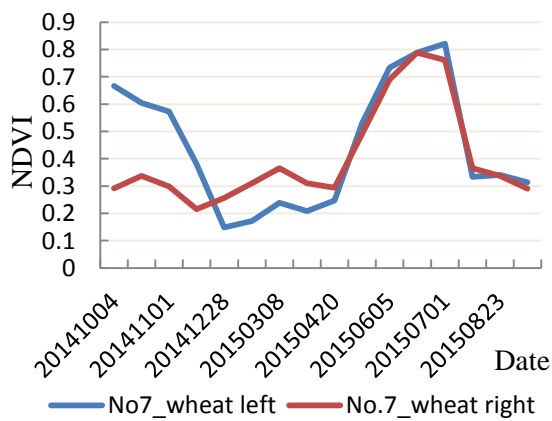


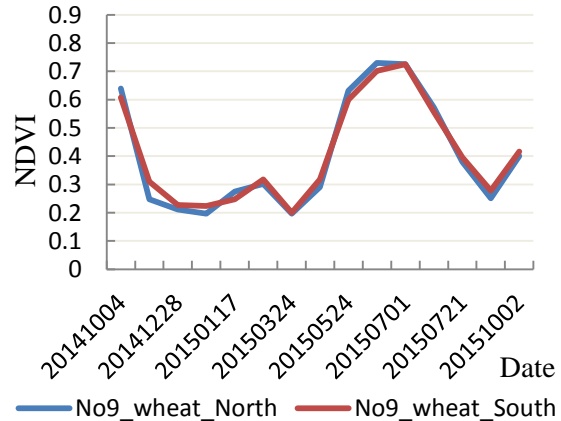
Figure 16 Daily rainfall data collected from Twente station, and the soil moisture data averaged from the 20 soil moisture network stations in Tewnte from October 2014 to September 2015.

### 6.3.2. NDVI for agricultural fields

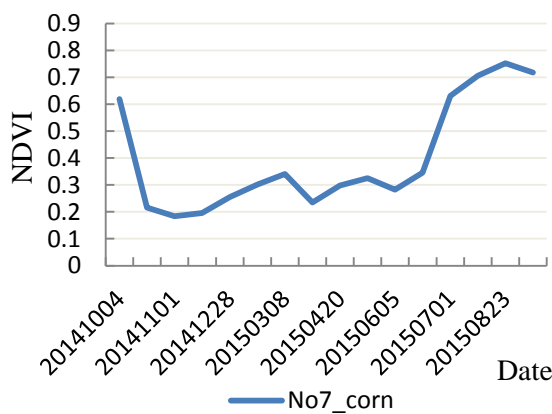
Figure 17 shows the NDVI for all observed field which were used to describe the relative density and biomass of vegetation. Furthermore, it is also used as an indicator for the agricultural activities (e.g., harvest). It can be seen from Figure 17, the same land cover type shows almost similar increasing and decreasing trends throughout the study period. According to Figure 17 (a,b), around the 20<sup>th</sup> April there is a markedly increasing of NDVI. Possible reason for the strong change may be due to the fact that wheat is start growing. In August, NDVI curves of wheat field decline significantly from the peaks (0.78) to the low point (0.32) which is related to the harvest. Although it is not very clear shown in the NDVI curve, it can be concluded that ploughing, seeding, would be done during October to January because the NDVI is kept low and changes slightly during the period. From October to January, the variation of NDVI in field No.7 is about 0.04, and there is almost no change in No.9 field. For corn field (Figure 17 c,d), the corn is growing faster from June and getting mature in October as the NDVI value changes from 0.31 to 0.75 and remain stable. In October, 2014, NDVI for No.7 corn field declines from 0.62 to 0.21. However, NDVI curve of No.8 field is much stable around 0.28. This is probably indicates that within study area corn was harvest at different time in 2014. Corn in No.7 field was harvest in October and corn in No.8 field had already been harvest before the October. Compared to the winter wheat and corn fields, NDVI of grassland is much higher. The average NDVI is 0.62 throughout the study period. Besides, NDVI curves of grassland increasing and decreasing more frequently which is probably due to the harvest as shown in Figure 17 (e,f).



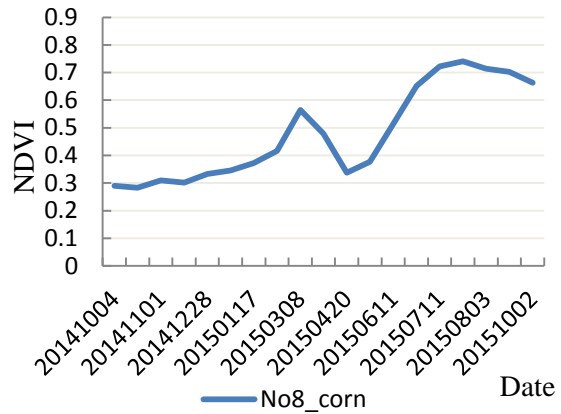
(a) No.7 Winter wheat field



(b) No.9 Winter wheat field



(c) No.7 Corn field



(d) No.8 Corn field

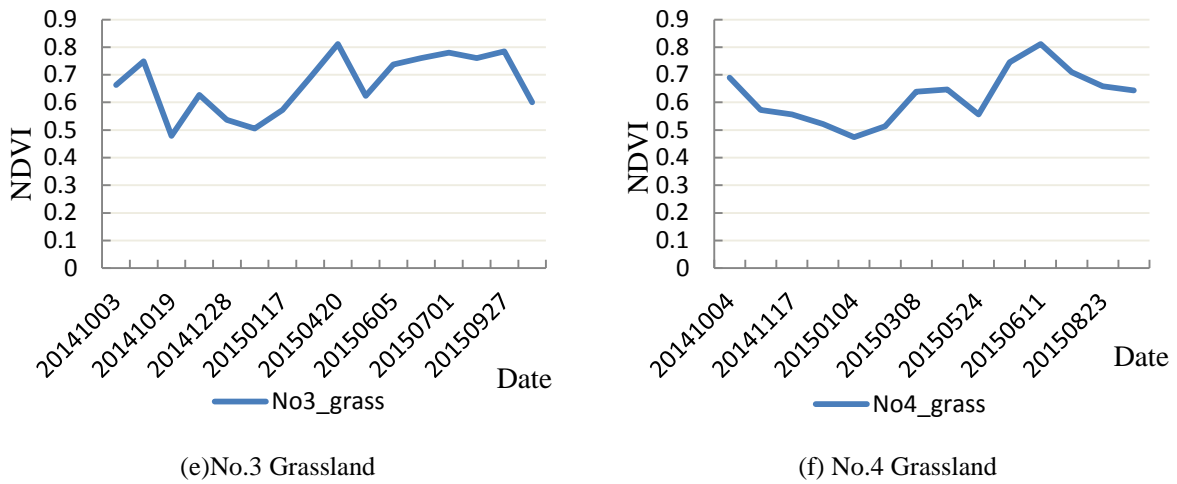
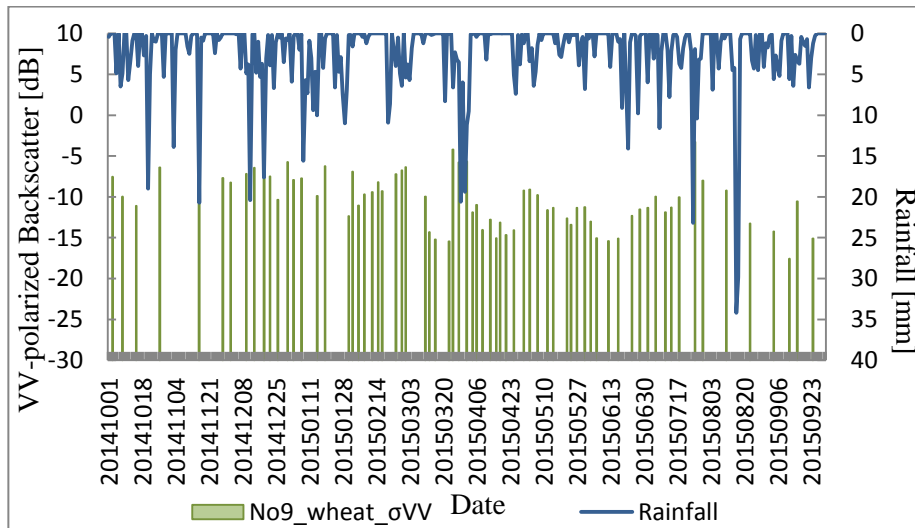


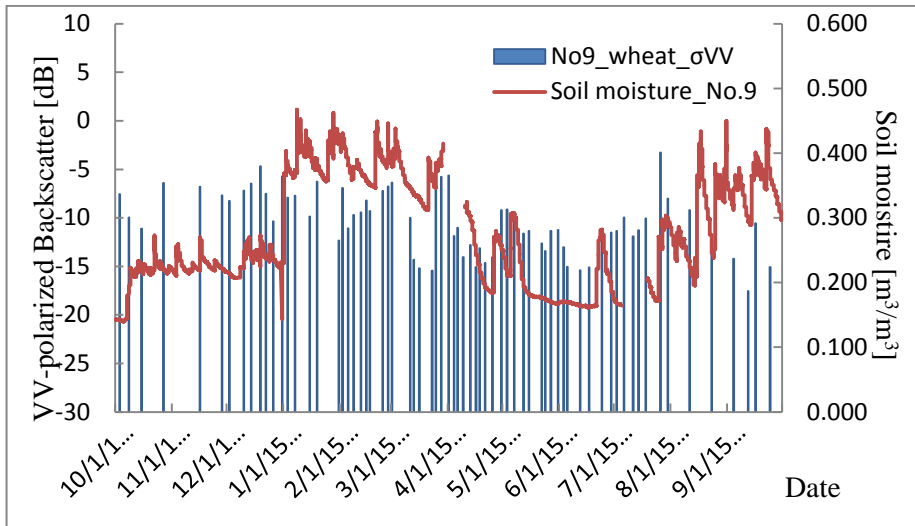
Figure 17 NDVI for corn fields, winter wheat field and grassland.

**6.3.3. Periodically standing water in winter wheat field**

According to Figure 15, fluctuation of backscatter from two non-adjacent winter wheat fields is quite different. The variation of backscatter in No.9 field is larger than No.7 field. The backscatter is also smaller than No.7 field. Particularly, it is clearly seen that the backscatter of No.9 field in September is much lower than the No.7. During the fieldwork period, No.7 and No.9 field had been visited on 24<sup>th</sup> September. Based on the observation, there was no standing water in the No.9 although the backscatter derived from No.9 north part field is much lower than No.7 field. In No.7 right part wheat field, standing water spread randomly mixing with the wheat-straw and grass as shown in Figure 8. While in No.9 field, the surface was smooth with sparse grass. Possible reason for the higher backscatter in No.7 field may be due to the wet soil moisture. The increase of the soil dielectric constant with water content leads to an enhanced signal return. In addition, rough surface also increases the backscatter signal observed by Sentinel-1.



(a) Rainfall with backscatter [dB] backscatter of No.9 wheat field



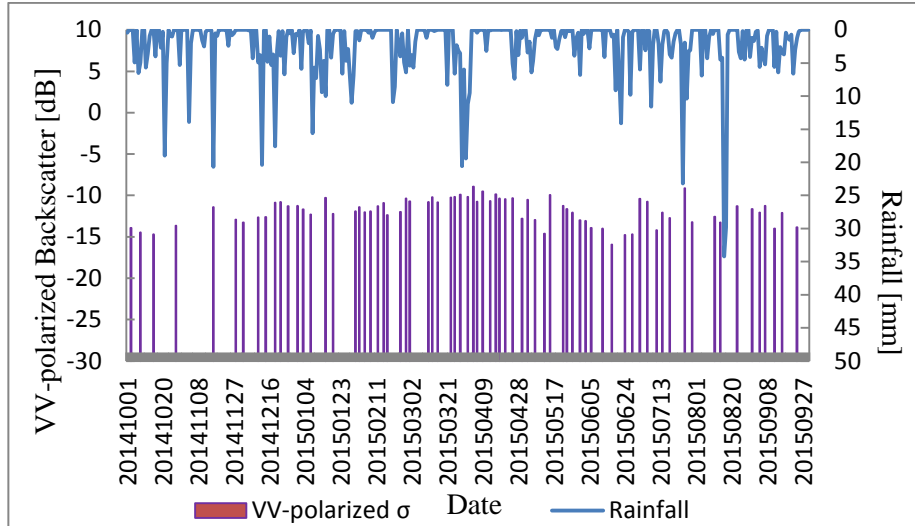
(b) Soil moisture with backscatter [dB] of No.9 wheat field

Figure 18 Soil moisture with backscatter of No.9 field and daily rainfall derived from Twente station.

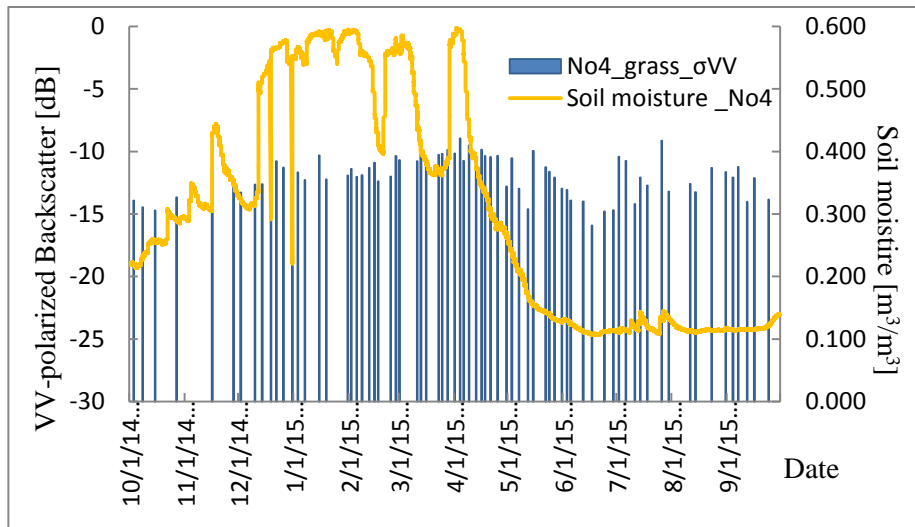
Figure 18 shows the soil moisture with backscatter of No.9 field and daily rainfall derived from Twente station. In general, soil moisture is in a good agreement with the rainfall. When there is a rainfall event or consist rainfall event, the soil moisture is increasing. According to Figure 18, backscatter around 12<sup>th</sup> June is relatively lower about -15.04 dB, however, the NDVI in June has reached the peak (0.72). Around 12<sup>th</sup> June, there is less rainfall, more importantly, the soil moisture during this period is lower than  $0.2 \text{ m}^3\text{m}^{-3}$ . Therefore, the low backscatter happens around 12<sup>th</sup> June is probably due to the low soil moisture instead of the standing water. Compared to vegetation biomass, soil moisture is the dominant factors in backscatter. In addition, in 23<sup>rd</sup> March, there is a sharply changes of backscatter and the backscatter decreases from -6.41 dB to -15.44 dB. Because the consistent rainfall events, the soil moisture in March is higher than  $0.3 \text{ m}^3\text{m}^{-3}$ . As the NDVI in March is much lower, the low backscatter in March probably due to the periodically standing water. On the other hand, the NDVI curve shows that the vegetation in No.9 winter wheat field is slightly increasing from the 24<sup>th</sup> March. The farmer activities like seeding could also affect the backscatter. Besides, there is decreasing trend of backscatter declines from -5.78 dB in 28<sup>th</sup> March to -15.43dB in 18<sup>th</sup> April. This is probably because the decreasing trend of rainfall during the same time.

#### 6.3.4. Periodically standing water in grassland

Figure 19 shows the soil moisture with backscatter of No.4 field and daily rainfall derived from Twente station. As shown in Table 6, the backscatter of grassland is much lower compared to the winter wheat and corn fields. However, NDVI of grassland is consistent and relatively higher throughout the study period as shown in Figure 17. The average NDVI of No.3 and No.4 field is 0.81 and 0.77, respectively. According to Figure 19, the backscatter trend is in a good agreement with the soil moisture curve before May, and the soil is extremely wet as the soil moisture is close to 0.6. It can be observed that the increasing trend of backscatter with increasing soil moisture in a densely biomass situations from January to May, 2015. However, during the same period, the backscatter is quite lower than other crop types. The possible reason for this may be due to the standing water, and it seems that vegetation biomass has less influent on backscatter changes.



(a) Rainfall with backscatter [dB] backscatter of No.9 wheat field



(b) Soil moisture with backscatter [dB] of No.4 grassland

Figure 19 Soil moisture with backscatter [dB] of No.4 field and daily rainfall derived from Twente station

## 7. CONCLUSION AND RECOMMENDATION

### 7.1. Conclusions

The main objective for this study aims to analyse Sentinel-1 data for its potential to map standing water in agricultural fields. A series of Sentinel-1 SAR images were used to detect the possible periodically standing water based on backscatter temporal variability and backscatter changes on field scale. Ancillary data, like soil moisture, rainfall, and NDVI were applied to verify the possible periodically standing water area. In addition, fieldwork has been done from 17<sup>th</sup> September 2015 to 2<sup>nd</sup> October 2015 in order to find the standing water in different kinds of agricultural fields. There are 6 fields had been visited including two grassland, two corn fields and two winter wheat fields. Only one winter wheat field (No.7 field) had obvious surface water. Standing water in one grassland (No.4 field) spread as mosaic under the thick grass. Moreover, the time of landscape changes and agricultural activities were recorded in order to analyse backscatter changes with respect to land surface conditions. The following conclusions are drawn from the analyses results.

- Standard deviation in dB and mean backscatter were calculated to show the backscatter temporal variation for a series SAR images. Open water body has the lowest backscatter (-18.44 dB VV-polarized backscatter) due to the specular reflection over the smooth water surface. It has the similar standard deviation with grassland. The standard deviation of open water body and grassland are 2.03 and 2.12, respectively. This is possibly due to waves on the water surface caused by the wind and the aquatic plant. Urban has the highest backscatter (-3.46 dB VV-polarized backscatter) and highest standard deviation (2.8) which probably with respect to the material of the building, cars on the road. Because of the volume scatter caused by the canopy and branches, forest has higher average backscatter (-7.49 dB VV-polarized backscatter). Temporal variability of forest (1.97) is the lowest because its typically constant over time and less affected by the surface conditions. Relatively higher standard deviation is found in agricultural fields, including corn fields (2.60) and winter wheat (2.57). Because of the seasonality of agricultural activity, soil moisture changes and weather conditions, corn fields and winter wheat have higher standard deviation compared to the grassland (2.12). In addition, the mean VV-polarized backscatter of winter wheat field is -8.25 dB which is similar to the corn field (-7.96 dB). These results show that multi-temporal backscatter observations can be used to classify the agricultural field from forest, urban, open water body and grassland. However, because of the effect of surface roughness, soil moisture and vegetation growth, winter wheat and corn field are difficult to distinguish.
- Changes in land surface conditions (e.g. soil moisture, vegetation biomass) due to atmospheric forcings, and human activities, like ploughing, seeding, and harvesting, affect the backscatter signal observed by Sentinel-1. Among all the possible influence factors, soil moisture is the dominant factors in backscatter change. The vegetation biomass in winter wheat fields and grassland is not a significant factor contributing to the backscatter changes.
- Based on the field-scale backscatter changes, standing water is difficult to delineate from the Sentinel-1 images due to the uncertainties. Those uncertainties include different surface conditions in each agricultural field, soil moisture, vegetation characteristics and agricultural activities. Those factors vary from temporal and spatial scale, like farming practices and atmospheric forcings.

### 7.2. Limitations and recommendations

- Due the ascending and descending of the sensor and the bug in the SNAP S1 tool box, there was a shift of the SAR images after the terrain correction. Then GCPs like roads cross points were used

to shift the images in order to overlay all the layers. However, by shift the image based on GCPs the accuracy has been a little bit decreased.

- The standing water area in observation is as much as  $10\text{ m} \times 5\text{ m}$  randomly distributed in the fields. However, the resolution of Sentinel-1 images is  $10\text{ m}$ . One problem would be that the standing water area is relatively small compared to the pixel size of the SAR observations.
- Limited number of standing water area has been found during the fieldwork period. Among 6 observed fields, only one winter wheat field has obvious standing water, and one grassland field has standing water underneath the densely grass. The number of observed standing water fields for analysis Sentinel-1 potential for mapping standing water is not enough. Therefore, the observation time should last longer in order to find enough observation standing water samples.
- In addition, in this study polygons were made for each observed field, which was used to extract the backscatter coefficient. Those regions of interesting were created in the center of the field in order to avoid the interference of the field boundary effect, such as tree canopy. Also, the backscatter of each observed field will be approximated by averaging calculation in order to decrease the effects of speckle. However, backscatter derived from a region will cause the signal of standing water mixed with other surface signals, which will add uncertainty to the result.
- Attention should be paid to the timing of the standing water and the interval time of the SAR images (e.g. when there will be standing water and its duration). The interval time of SAR images in this study very from 2 to 11 days.
- Among the study area, agricultural activities like the ploughing, seeding, harvest start at different time which depends on the crop type and farmer's time schedule. Therefore, we have limited information about the field conditions, for example, surface roughness, grass cover, what had been left after the harvest. Because those factors would affect the signal of observation. In order to better understand the backscatter changes, more information about the crop and landscape in the field should be collected.
- Larger area of standing water should be found to reduce the effect of grass, roughness soil around the water.
- More quantitative measurements of the standing water area should be collected for the further validation



## LIST OF REFERENCES

---

- ASAR - Earth Online - ESA. (n.d.). Retrieved August 26, 2015, from <https://earth.esa.int/web/guest/missions/esa-operational-eo-missions/envisat/instruments/asar>
- Attema, E., Davidson, M., Snoeij, P., Rommen, B., Floury, N., & Agency, E. S. (2009). SENTINEL-1 MISSION OVERVIEW, 36–39.
- Bazi, Y., Bruzzone, L., & Melgani, F. (2007). Image thresholding based on the EM algorithm and the generalized Gaussian distribution. *Pattern Recognition*, *40*(2), 619–634. <http://doi.org/10.1016/j.patcog.2006.05.006>
- Berning, C., Viljoen, M. F., & Du Plessis, L. A. (2000). Loss functions for sugar-cane: Depth and duration of inundation as determinants of extent of flood damage. *Water SA*, *26*(4), 527–530.
- Bruzzone, L., Marconcini, M., Wegmüller, U., & Wiesmann, A. (2004). An advanced system for the automatic classification of multitemporal SAR images. *IEEE Transactions on Geoscience and Remote Sensing*, *42*(6), 1321–1334. <http://doi.org/10.1109/TGRS.2004.826821>
- Cloude, S. (2009). *Polarisation: Applications in Remote Sensing*. Retrieved from <https://books.google.com/books?hl=zh-CN&lr=&id=c67UPCcbfHUC&pgis=1>
- Dente, L., Su, Z., & Wen, J. (2012). Validation of SMOS soil moisture products over the Maqu and Twente Regions. *Sensors*, *12*(8), 9965–9986. <http://doi.org/10.3390/s120809965>
- Dente, L., Vekerdy, Z., Su, Z., & Ucer, M. (2011). *Soil Moisture and Soil Temperature Monitoring Network*.
- Di Baldassarre, G., Schumann, G., & Bates, P. D. (2009). A technique for the calibration of hydraulic models using uncertain satellite observations of flood extent. *Journal of Hydrology*, *367*(3-4), 276–282. <http://doi.org/10.1016/j.jhydrol.2009.01.020>
- Dostálová, A., Doubková, M., Sabel, D., Bauer-Marschallinger, B., & Wagner, W. (2014). Seven Years of Advanced Synthetic Aperture Radar (ASAR) Global Monitoring (GM) of Surface Soil Moisture over Africa. *Remote Sensing*, *6*, 7683–7707. <http://doi.org/10.3390/rs6087683>
- ERS overview / Observing the Earth / Our Activities / ESA. (n.d.). Retrieved August 26, 2015, from [http://www.esa.int/Our\\_Activities/Observing\\_the\\_Earth/ERS\\_overview](http://www.esa.int/Our_Activities/Observing_the_Earth/ERS_overview)
- Giustarini, L., Hostache, R., Matgen, P., Schumann, G. J., Bates, P. D., & Mason, D. C. (2013). A Change Detection Approach to Flood Mapping in Urban Areas Using TerraSAR-X. *IEEE Transactions on Geoscience and Remote Sensing*, *51*(4), 2417–2430. <http://doi.org/10.1109/TGRS.2012.2210901>
- Gstaiger, V., Huth, J., Gebhardt, S., Wehrmann, T., & Kuenzer, C. (2012). Multi-sensoral and automated derivation of inundated areas using TerraSAR-X and ENVISAT ASAR data. *International Journal of Remote Sensing*, *33*(22), 7291–7304. <http://doi.org/10.1080/01431161.2012.700421>
- Henry, J. - B., Chastanet, P., Fellah, K., & Desnos, Y. - L. (2006). Envisat multi - polarized ASAR data for flood mapping. *International Journal of Remote Sensing*, *27*(10), 1921–1929. <http://doi.org/10.1080/01431160500486724>
- Hostache, R., Matgen, P., & Wagner, W. (2012). Change detection approaches for flood extent mapping: How to select the most adequate reference image from online archives? *International Journal of Applied Earth Observation and Geoinformation*, *19*(1), 205–213. <http://doi.org/10.1016/j.jag.2012.05.003>

- Kuenzer, C., Guo, H., Huth, J., Leinenkugel, P., Li, X., & Dech, S. (2013). Flood mapping and flood dynamics of the mekong delta: ENVISAT-ASAR-WSM based time series analyses. *Remote Sensing*, 5(2), 687–715. <http://doi.org/10.3390/rs5020687>
- Matgen, P., Hostache, R., Schumann, G., Pfister, L., Hoffmann, L., & Savenije, H. H. G. (2011). Towards an automated SAR-based flood monitoring system: Lessons learned from two case studies. *Physics and Chemistry of the Earth*, 36(7-8), 241–252. <http://doi.org/10.1016/j.pce.2010.12.009>
- Mladenova, I. E., Jackson, T. J., Bindlish, R., & Hensley, S. (2012). Incidence Angle Normalization of Radar Backscatter Data. *Geoscience and Remote Sensing, IEEE Transactions on*, 51(3), 1791–1804. <http://doi.org/10.1109/TGRS.2012.2205264>
- Mtamba, J., van der Velde, R., Ndomba, P., Zoltán, V., & Mtaló, F. (2015). Use of Radarsat-2 and Landsat TM Images for Spatial Parameterization of Manning's Roughness Coefficient in Hydraulic Modeling. *Remote Sensing*, 7(1), 836–864. <http://doi.org/10.3390/rs70100836>
- O'Grady, D., Leblanc, M., & Gillieson, D. (2013). Relationship of local incidence angle with satellite radar backscatter for different surface conditions. *International Journal of Applied Earth Observation and Geoinformation*, 24, 42–53. <http://doi.org/10.1016/j.jag.2013.02.005>
- Pulvirenti, L., Chini, M., Pierdicca, N., Guerriero, L., & Ferrazzoli, P. (2011). Flood monitoring using multi-temporal COSMO-SkyMed data: Image segmentation and signature interpretation. *Remote Sensing of Environment*, 115(4), 990–1002. <http://doi.org/10.1016/j.rse.2010.12.002>
- Pulvirenti, L., Pierdicca, N., Chini, M., & Guerriero, L. (2011). An algorithm for operational flood mapping from Synthetic Aperture Radar (SAR) data using fuzzy logic. *Natural Hazards and Earth System Science*, 11(2), 529–540. <http://doi.org/10.5194/nhess-11-529-2011>
- Schlaffer, S., Matgen, P., Hollaus, M., & Wagner, W. (2015). Flood detection from multi-temporal SAR data using harmonic analysis and change detection. *International Journal of Applied Earth Observation and Geoinformation*, 38, 15–24. <http://doi.org/10.1016/j.jag.2014.12.001>
- Schumann, G., Di Baldassarre, G., & Bates, P. D. (2009). The utility of spaceborne radar to render flood inundation maps based on multialgorithm ensembles. *IEEE Transactions on Geoscience and Remote Sensing*, 47(8), 2801–2807. <http://doi.org/10.1109/TGRS.2009.2017937>
- Schumann, G. J.-P., & Moller, D. K. (2015). Microwave remote sensing of flood inundation. *Physics and Chemistry of the Earth, Parts A/B/C*. <http://doi.org/10.1016/j.pce.2015.05.002>
- Sentinel-1 Team. (2013). *Sentinel-1 User handbook*. <http://doi.org/GMES-S1OP-EOPG-TN-13-0001>
- Ticehurst, C. J., Dyce, P., & Guerschman, J. P. (2009). Using passive microwave and optical remote sensing to monitor flood inundation in support of hydrologic modelling. *18th World IMACS / MODSIM Congress, Cairns, Australia*, (July), 3747–3753. Retrieved from <http://mssanz.org.au/modsim09>
- Torres, R., Snoeij, P., Geudtner, D., Bibby, D., Davidson, M., Attema, E., ... Rostan, F. (2012). GMES Sentinel-1 mission. *Remote Sensing of Environment*, 120, 9–24. <http://doi.org/10.1016/j.rse.2011.05.028>
- Townsend, P. a., & Walsh, S. J. (1998). Modeling floodplain inundation using an integrated GIS with radar and optical remote sensing. *Geomorphology*, 21(3-4), 295–312. [http://doi.org/10.1016/S0169-555X\(97\)00069-X](http://doi.org/10.1016/S0169-555X(97)00069-X)

Velde, R. Van Der, Salama, M. S., Eweys, O. A., Wen, J., & Wang, Q. (2014). Active / Passive Microwave Observations Over the East of the Netherlands, 1–18.